Brain, Behavior, and Immunity 89 (2020) 67–86

Contents lists available at ScienceDirect

Brain, Behavior, and Immunity

journal homepage: www.elsevier.com/locate/ybrbi

CD8$^+$ T-cells infiltrate Alzheimer's disease brains and regulate neuronal- and synapse-related gene expression in APP-PS1 transgenic mice

M.S. Unger[a,b], E. Li[a,b], L. Scharnagl[a,b], R. Poupardin[b,c], B. Altendorfer[a,b], H. Mrowetz[a,b], B. Hutter-Paier[d], T.M. Weiger[e], M.T. Heneka[f,g], J. Attems[h], L. Aigner[a,b,i,*]

[a] Institute of Molecular Regenerative Medicine, Paracelsus Medical University, Salzburg, Austria
[b] Spinal Cord Injury and Tissue Regeneration Center Salzburg (SCI-TReCS), Paracelsus Medical University, Salzburg, Austria
[c] Experimental and Clinical Cell Therapy Institute, Paracelsus Medical University, Salzburg, Austria
[d] QPS Austria GmbH, Parkring 12, 8074 Grambach, Austria
[e] Department of Biosciences, University of Salzburg, Salzburg, Austria
[f] German Center for Neurodegenerative Diseases (DZNE), Bonn, Germany
[g] Department of Neurodegenerative Diseases and Geriatric Psychiatry, University Hospital of Bonn, Bonn, Germany
[h] Translational and Clinical Institute, Newcastle University, Newcastle upon Tyne, UK
[i] Austrian Cluster for Tissue Regeneration, Austria

ARTICLE INFO

Keywords:
CD8$^+$ T-cells
Alzheimer's disease
RNAseq
Synapse
Npas4
Arc

ABSTRACT

Neuroinflammation is a major contributor to disease progression in Alzheimer's disease (AD) and is characterized by the activity of brain resident glial cells, in particular microglia cells. However, there is increasing evidence that peripheral immune cells infiltrate the brain at certain stages of AD progression and shape disease pathology. We recently identified CD8$^+$ T-cells in the brain parenchyma of APP-PS1 transgenic mice being tightly associated with microglia as well as with neuronal structures. The functional role of CD8$^+$ T-cells in the AD brain is however completely unexplored. Here, we demonstrate increased numbers of intra-parenchymal CD8$^+$ T-cells in human AD post-mortem hippocampus, which was replicated in APP-PS1 mice. Also, aged WT mice show a remarkable infiltration of CD8$^+$ T-cells, which was more pronounced and had an earlier onset in APP-PS1 mice. To address their functional relevance in AD, we successfully ablated the pool of CD8$^+$ T-cells in the blood, spleen and brain from 12 months-old APP-PS1 and WT mice for a total of 4 weeks using an anti-CD8 antibody treatment. While the treatment at this time of disease stage did neither affect the cognitive outcome nor plaque pathology, RNAseq analysis of the hippocampal transcriptome from APP-PS1 mice lacking CD8$^+$ T-cells revealed highly altered neuronal- and synapse-related gene expression including an up-regulation for neuronal immediate early genes (IEGs) such as the Activity Regulated Cytoskeleton Associated Protein (*Arc*) and the Neuronal PAS Domain Protein 4 (*Npas4*). Gene ontology enrichment analysis illustrated that the biological processes *"regulation of neuronal synaptic plasticity"* and the cellular components *"postsynapses"* were over-represented upon CD8$^+$ T-cell ablation. Additionally, Kegg pathway analysis showed up-regulated pathways for "*calcium signaling*", "*long-term potentiation*", "*glutamatergic synapse*" and "*axon guidance*". Therefore, we conclude that CD8$^+$ T-cells infiltrate the aged and AD brain and that brain CD8$^+$ T-cells might directly contribute to neuronal dysfunction in modulating synaptic plasticity. Further analysis will be essential to uncover the exact mechanism of how CD8$^+$ T-cells modulate the neuronal landscape and thereby contribute to AD pathology.

1. Introduction

Alzheimer's disease (AD) is the most common form of dementia and characterized by an age-related neurodegeneration of the brain leading to a progressive cognitive decline (reviewed in Goedert and Spillantini 2006). Typical histopathological hallmarks of AD are amyloid-beta plaques and neurofibrillary tangles (reviewed in Gotz et al., 2007; Meadowcroft et al., 2009; Philipson et al., 2010; Selkoe and Hardy, 2016; Serrano-Pozo et al., 2011). However, besides these classical characteristics, neuroinflammation is described as an important contributor to AD pathology (reviewed in Heneka et al., 2015; Heppner et al., 2015; Wyss-Coray, 2006).

Neuroinflammation is primarily related to microglia, which are the brains resident immune cells and key players in inflammatory processes

* Corresponding author at: Institute of Molecular Regenerative Medicine, Paracelsus Medical University, Strubergasse 21, 5020 Salzburg, Austria.
E-mail address: ludwig.aigner@pmu.ac.at (L. Aigner).

https://doi.org/10.1016/j.bbi.2020.05.070
Received 17 December 2019; Received in revised form 25 May 2020; Accepted 26 May 2020
Available online 29 May 2020

of the central nervous system (CNS) (reviewed Fu et al., 2014; Kettenmann et al., 2011). They are mediating chronic neuroinflammation and aggravation in AD pathology (reviewed in (Heppner et al., 2015; Krabbe et al., 2013; Wyss-Coray and Rogers, 2012). Yet, a diversity of peripheral immune cells including macrophages (reviewed in Gate et al., 2010; Theriault et al., 2015; and Prokop et al., 2015), neutrophils (Zenaro et al., 2015) and lymphocytes (reviewed in Baruch and Schwartz, 2013; and Baruch et al., 2015; Ferretti et al., 2016; Marsh et al., 2016) are known to infiltrate the brains of AD transgenic mice. Especially lymphocytes are heavily discussed to be involved in AD pathology (reviewed in Jevtic et al., 2017). Specifically, T-lymphocytes are detected in the aging rodent brain (Korin et al., 2017; Ritzel et al., 2016), in excessive numbers in human AD post-mortem specimen (Merlini et al., 2018; Rogers et al., 1988; Togo et al., 2002) as well as in amyloid plaque diseased brain regions from transgenic AD mice (Ferretti et al., 2016; and reviewed in Jevtic et al., 2017). T-cells in the brains of transgenic AD mice have been identified as $CD3^+/CD4^+$ T-helper cells and as $CD3^+/CD8^+$ cytotoxic T-cells (Ferretti et al., 2016; Unger et al., 2018a; Unger et al., 2018b). Apparently, in AD post-mortem brains $CD3^+$ T-cells correlate with Tau but not with amyloid plaque pathology (Merlini et al., 2018), and due to conflicting results the functional relevance of $CD3^+$ T-cells in AD is unclear (Baruch et al., 2015; Dansokho et al., 2016; Marsh et al., 2016). Surprisingly, although $CD8^+$ T-cells outline $CD4^+$ T-cells in numbers in the brain (Ferretti et al., 2016; Korin et al., 2017), a putative role of $CD8^+$ T-cells in AD was so far largely ignored. Only recently, Gate D. and us could demonstrate that a specific $CD8^+$ T-cell population (T_{EMRA} T-cells) was clonally expanded in the CSF and elevated in the blood of AD patients (Gate et al., 2020). In addition, we demonstrated that $CD3^+/CD8^+$ T-cell lymphocytes infiltrated the human AD brains and brains of transgenic mice with plaque pathology, and that these cells are in tight contact to microglia as well as to neuronal structures (Gate et al., 2020; Unger et al., 2018b). The functional role of $CD8^+$ T-cells in the AD brain is completely unknown.

Here, we first investigated the temporal profile of $CD8^+$ T-cell infiltration into the brain parenchyma of APP-PS1 transgenic mice, i.e. an amyloid plaque mouse model of AD, in relation to the age of animals and stage of pathology. Additionally, we analysed the presence of intraparenchymal $CD8^+$ T-cells in the brains of AD patients compared to age-matched healthy controls. Further, we ablated $CD8^+$ T-cells from WT and from APP-PS1 transgenic mice and performed unbiased transcriptomic analysis of the hippocampus revealing remarkable changes in gene expression related to neuronal and synaptic functions.

2. Material & methods

2.1. Animals and $CD8^+$ T-cell ablation experiment

Female and male APP Swedish PS1 dE9 mice (Jankowsky et al., 2001; Jankowsky et al., 2004) expressing a chimeric mouse/human mutant amyloid precursor protein (Mo/HuAPP695swe) and a mutant human presenilin 1 (PS1-dE9) both directed to CNS neurons under the prion protein promoter were used (available by Jackson Laboratory, http://www.jax.org/strain/005864). Mice were housed at the Paracelsus Medical University Salzburg in groups under standard conditions at a temperature of 22 °C and a 12 h light/dark cycle with ad libitum access to standard food and water. Animal care, handling, genotyping and experiment were approved by local ethical committees (BMBWF-66.019/0005-V/3b/2018). Animal breeding was done under special pathogen free (SPF) conditions and mice were transferred to non-SPF conditions for experimental ablation of $CD8^+$ T-cells and behavioural tests.

For the analysis of $CD8^+$ T-cell numbers in the brain over time, APP Swedish PS1 dE9 (herein abbreviated as APP-PS1) and breeding derived age-matched non-transgenic mice (herein named WT) of different ages were used (3 months, 10 months, 12–13 months, 18–19 months and 25–26 months old). For the in vivo experiment, 12-months old APP-PS1 and WT mice were used. Animals were treated for a total of 4 weeks with an anti-CD8a antibody (clone 2.43 #BE0061, BioXCell), a respective isotype control antibody (rat IgG2b clone LTF-2 #BE0090, BioXCell) or PBS. Mice were injected i.p. for 3 consecutive days and additionally on the 5th day, followed by 2 injections per week for a total of 10 injections á 0.8 mg of respective antibody. PBS treated mice received 100 µL of PBS. For the in vivo experiment animals of mixed gender were used and the sex ratio in the experimental groups for all used animals was as follows: WT + PBS: 4 male, 5 female; WT + isotype control: 4 male, 9 female; WT + anti-CD8: 4 male, 7 female; APP-PS1 + PBS: 4 male, 5 female; APP-PS1 + isotype control: 5 male, 6 female; APP-PS1 + anti-CD8: 8 male, 5 female. In the first 3 weeks of treatment mice were fixed in a restrainer and blood was drawn from vena saphena once per week to monitor $CD8^+$ T-cell ablation (see Fig. 2A). Small volumes of blood (about 20–50 µL) were transferred to a drop of PBS containing 0.1 M EDTA (Promega) for flow cytometry analysis. T-cell ablation was additionally controlled at perfusion day.

Brains from 6 months old TMHT (Flunkert et al., 2013) and hTau Tau transgenic mice (Andorfer et al., 2003) were generously provided by the contract research organization QPS Austria (http://qpsneuro.com/in-vivo-services/animal-models/tau-tg-mouse-models).

2.2. Behavior test: Morris water maze

Behavior tests were performed in a special animal experiment room at the animal facility of the Paracelsus Medical University Salzburg under constant light and environmental conditions. In the 4th week of anti-CD8 treatment the Morris Water Maze (MWM) behavioral test was performed as previously published (Rotheneichner et al., 2017; Unger et al., 2018b). The test was conducted at the same daytime and camera tracked using EthoVision tracking system (EthoVision XT 9.0.726, Noldus).

In short, MWM is a standard cognitive behavior test for spatial learning and memory function (Bromley-Brits et al., 2011; Morris, 1981). MWM was performed on 6 consecutive days. The maze consisted of a 108 cm round white pool that was filled with 22 °C warm water up to 1 cm above a transparent plastic platform that was placed in the southwest quadrant of the arena. The 10 × 10 cm platform was hidden under the water surface and was visually not detectable for the animals. Every mouse was put in the maze for 60 s and the activity (e.g. swim speed, time spent in the arena zones and the distance moved) until the mouse reached the platform was recorded. If the mouse did not reach the platform after 60 s, it was manually cued to the platform for orientation before it was taken out of the maze. Each mouse had to perform 4 trials per day for 5 consecutive days. Every trial per day started at 4 different visually marked entry points (square, triangle, circle, moon) and the entry points to the maze were randomly shuffled over the 5 days to avoid any learning effects caused by memory of the entry point. After each trial the animals had one hour to rest before starting a new trial. On the 1st day the platform was emphasized with a flag to help the mice to find the platform and the data from day 1 were therefore excluded from the analysis. On the 6th day the mice were additionally tested for spatial memory by removing the platform. The mice had 60 s time to search the original spatial location of the platform. For behavior testing n = 8–10 animals per group were used.

2.3. Perfusion and tissue sectioning

After 4 weeks of treatment mice were anesthetized by intraperitoneal injection of a ketamine (20.5 mg/ml, Richter Pharma), xylazine (5.36 mg/ml, Chanelle) and acepromacine (0.27 mg/ml, VANA GmbH) mixture. Afterwards their thoracic cavity was opened with an incision caudal to the sternum. Blood was drawn from the heart for subsequent isolation of sera and stored at −80 °C. A small volume

(50 µL) of total blood was collected in 20 µL PBS containing 0.1 M EDTA. Afterwards animals were manually perfused through the left ventricle with 0.9% NaCl solution for histology or for subsequent flow cytometry analysis of brain homogenates ice cold HBSS containing 15 mM HEPES (all from Thermofisher) and 0.5% glucose (Sigma) was used to wash out the blood. Mice were decapitated and brains were extracted from the skull. One total brain hemisphere was immersed in 4% paraformaldehyde (in 0.1 M sodium phosphate solution, pH = 7.4) for fixation over night before being washed in PBS and transferred into 30% sucrose for cryoprotection. Similarly, half spleens were fixed with 4% paraformaldehyde for up to 4 h, rinsed in PBS and transferred into 30% sucrose. When fully soaked with sucrose brain hemispheres and spleens were cut in 40 µm slices on dry ice using a sliding microtome (Leika) dividing one brain hemisphere in representative 10^{ths} of the brain. Sections were stored at −20 °C in cryoprotectant solution (ethylene glycol, glycerol, 0.1 M sodium phosphate buffer pH 7.4, 1:1:2 by volume). The other brain hemisphere was further processed for RNA isolation or flow cytometry analysis.

2.4. Flow cytometry analysis

Brain: For analysis of brain T-cells and microglia/macrophages one total brain hemisphere (including brainstem and cerebellum) per mouse was mechanically chopped with a razor blade and homogenized in 2 mL ice cold HBSS with 15 mM HEPES (all from Thermofisher), 0.5% glucose (Sigma) and RNAsin (1:250, Promega) using a glass homogenizer. Cells were passed through a 100 µm cell strainer and rinsed two times with 2 mL ice cold HBSS (with 15 mM HEPES and 0.5% glucose). Cell suspensions were centrifuged at 340 g for 7 min. at 4 °C. Myelin was removed by resuspending the cell pellet in 30% percoll (Sigma) solution and centrifugation at 950 g for 20 min. at 4 °C. Supernatant was carefully removed and pellets containing cells of interest were diluted in HBSS followed by centrifugation at 300 g for 10 min at 4 °C. Pellets were resuspended in PBS containing fixable viability dye (1:2000, eBioscience #65-0865) for 3 min. at RT and transferred to round-bottom polystyrene tubes (Corning). After centrifugation for 5 min. at 300 g, cell pellets were dissolved in FACS buffer (PBS with 2% BSA and 2 mM EDTA) containing Rat Anti-Mouse CD16/CD32 Fc-Block (1:100, BD Biosciences, #553141) for 5 min. at RT. Samples were again centrifuged at 300 g for 5 min. and pellets dissolved in FACS buffer containing primary fluorescent labelled antibodies. Antibody incubation was performed for 15 min. at RT. Samples were washed in FACS buffer two times and centrifuged at 400 g for 5 min. Finally, cell pellets were resuspended in 500 µL FACS buffer with RNAsin (1:250, Promega #N2115) and filtered with a 30 µm cell strainer followed by flow cytometric analysis using LSR Fortessa flow cytometer (BD) with BD FACSDiva software (8.0.1, BD). Following primary antibodies were used: CD11b-PE (1:100, eBioscience, 12-0112-82), CD45-PE/Cy7 (1:100, BioLegend #103114), CD3-APC (1:100, eBioscience #17-0032), CD4-eFluor450 (1:100, eBioscience #48-0041), CD8b-FITC (1:100, eBioscience #11-0083-82).

Single stains were performed for compensations with PBMCs collected from whole mouse blood drawn from the heart for CD3-APC, CD4-eFluor450 and CD8b-FITC and with brain lysate for CD11b-PE, CD45-PE/Cy7 and viability dye eFluor780. As gating strategy cells of interest were taken and cell doublets were discriminated. Single cells negative for Viability Dye eFluor780 were counted as living cells and gated for CD3-APC and CD45-PE/Cy7 expression. The T-cell population was further analysed for CD4-eFluor450 and CD8b-FITC expression. Total cell numbers for $CD3^+$, $CD3^+/CD4^+$ and $CD3^+/CD8^+$ were measured and calculated for $1x10^5$ living cells in each sample. Similarly, single-living $CD11b^+$ cells were gated for $CD11b^+/CD45^{low}$ or $CD11b^+/CD45^{high}$ cells to discriminate between microglia and CNS/peripheral macrophages as published by several groups (Becher and Antel, 1996; Bennett et al., 2016; Ford et al., 1995; Korin et al., 2017). Total cell numbers for $CD11b^+/CD45^{low}$, and $CD11b^+/CD45^{high}$ were measured from total brain hemispheres and calculated for 1×10^5 living cells in each sample. Flow cytometry data analysis of brain tissue and graphs were done with Kaluza analysis software (1.3 Beckman Coulter).

Blood: For weekly monitoring of the $CD8^+$ T-cell ablation in the blood, small volumes of blood were collected from the vena saphena, pre-blocked with Rat Anti-Mouse CD16/CD32 Fc-Block (1:100, BD Biosciences, #553141) and directly stained for CD3-APC (1:100, eBioscience, #17-0032), CD4-PerCP (1:100, BioLegend, #100537) and CD8b-FITC (1:200, eBioscience, #11-0083-82) for 30 min at RT in the dark. Afterwards red blood cells were lysed (RBC lysis buffer, eBiosciences, #00-4300) and samples were measured with BD Accuri C6 Plus (BD Biosciences). Compensation values were loaded from the quality control according to manufacturer's instructions. Cells of interest (lymphocytes) were gated for CD3-APC expression, plotted for CD4-PerCP and CD8b-FITC and the cell numbers from the frequencies of $CD4^-/CD8^-$, $CD4^+/CD8^-$, $CD4^-/CD8^+$ and $CD4^+/CD8^+$ were measured (BD CSampler Plus software v1.0.23.1, BD Biosciences). Total respective cell numbers were calculated for 1.5×10^4 $CD3^+$ T-cells in each sample. Additionally, the CD4:CD8 ratio ($CD4^+/CD8^-$:$CD4^-/CD8^+$) and percentage of $CD3^+$ T-cells in the cells of interest gate was analysed and compared between the groups. To avoid any false negative results in flow cytometry analysis due to the injection of the anti-CD8a antibody, a non-competing clone as detection antibody recognizing only the CD8b antigen was used as previously published by others (Laky and Kruisbeek, 2016). Our data represent frequencies without the use of counting beads.

2.5. Fluorescence immunohistochemistry (IHC)

Fluorescence Immunohistochemistry of mouse tissue was performed on free-floating sections as previously described (Marschallinger et al., 2015; Unger et al., 2016). In short, antigen retrieval was performed depending on the used primary antibody by steaming the sections for 15–20 min. in citrate buffer (pH = 6.0, Sigma). After blocking unspecific antibody binding sites sections were incubated on a shaker over night at RT with following primary antibodies: rat anti-CD8a (1:100, eBioscience, clone 4SM16), rabbit anti-CollagenIV (1:500, Abcam), goat anti-CollagenIV (1:300, Millipore), mouse anti-pTau/AT180 (1:100, Invitrogen), rabbit anti-NeuN (1:200, Cell Signaling), chicken anti-GFAP (1:2000, Abcam), goat anti-Olig2 (1:300, R&D Systems), rabbit anti-Iba1 (1:1000, Abcam), goat anti-Iba1 (1:500, Abcam), rabbit anti-Arc (1:100, Abcam), rabbit anti-Npas4 (1:100, Novus Biologicals) and guinea pig anti-NeuN (1:750, Millipore). For the transcription factor Npas4 a nucleus staining protocol with 2 days of primary antibody incubation was performed as previously published (Unger et al., 2016). Sections were extensively washed in PBS and incubated for 3 h at RT in appropriate fluorescent-labelled secondary antibodies (Invitrogen or Jackson ImmunoResearch, all diluted 1:1000).

Nucleus counterstaining was performed with 4′,6-diamidino-2-phenylindole dihydrochloride hydrate (DAPI 1 mg/mL, 1:2000, Sigma). For amyloid-beta plaque staining, ThioflavinS (1 mg/mL, 1:625, Sigma) was added to the secondary antibody solution. Tissue sections were additionally treated with 0.2% Sudan Black (Sigma) in 70% ethanol for 1–2 min to reduce the autofluorescence in tissue from old animals (Schnell et al., 1999). After this treatment the sections were extensively washed in PBS and mounted onto microscope glass slides (Superfrost Plus, Thermo Scientific). Brain sections were cover slipped semi-dry in ProLong Gold Antifade Mountant (Life technologies) or Fluorescence Mounting Medium (Dako).

To detect remaining $CD8^+$ T-cells in the spleen or brain, a rat anti-CD8a antibody from a different clone as the injection antibody was used. Additionally, fluorescence labelled secondary donkey anti-rat antibodies were used to detect treatment resistant T-cells in anti-CD8a antibody injected animals.

2.6. Human FFPE tissue

We used 7 μm hippocampal sections from formalin-fixed paraffin embedded brain samples which were obtained from the Newcastle Brain Tissue Resource (NBTR) in accordance with Newcastle University ethics board and ethical approval awarded by The Joint Ethics Committee of Newcastle and North Tyneside Health Authority (reference: 08/H0906/136). Irrespective of clinical diagnoses, all brains underwent neuropathological examination according to a routine protocol that uses standardized neuropathological scoring/grading systems, including neurofibrillary tangle (NFT) Braak staging (Braak and Braak, 1991; Braak et al., 2006), Consortium to Establish a Registry for Alzheimer's Disease (CERAD) scores (Mirra et al., 1991), Newcastle/McKeith Criteria for Lewy body disease (McKeith et al., 2005), National Institute on Aging – Alzheimer's Association (NIA-AA) guidelines (Montine et al., 2012) and Thal phases of amyloid β deposition (Thal et al., 2002).

Our study group consisted of 8 AD cases which showed NFT Braak stage V-VI and fulfilled the criteria for high AD neuropathological change according to NIA-AA guidelines (Montine et al., 2012) and besides classical AD pathology (i.e., neurofibrillary tangles, amyloid plaques, and neuritic plaques) did not show any other pathology (e.g. Lewy bodies, TDP-43 positive intracellular inclusions) in the hippocampus. As controls we used 5 cases with NFT Braak stages 0 to III, which showed no or only very limited amounts of amyloid pathology in the hippocampus.

Human samples were immunohistologically stained as follows: after deparaffinization and rehydration of brain slides, extended antigen retrieval was performed for 2 h in citrate buffer (pH = 6.0, Sigma) using a steamer. Subsequently samples were H_2O_2 quenched with 0.3% H_2O_2, blocked and slides were incubated in primary antibody over night at RT in a humid chamber. The following primary antibody was used: rabbit anti-human CD8 antibody 1:300 (108R-16; Cell Marque). On the next day slides were washed and incubated with biotinylated secondary goat anti-rabbit antibody (1:500, Vector Lab BA-1000) for 1 h at RT. Signals were increased using the Vectastain ABC Hrp Kit (Vector) for 1 h according to manufacturer's instructions. After washing, sections were transferred to 3,3′-Diaminobenzidin (DAB) using the Peroxidase Substrate Kit (Vector) following manufacturer's instructions (without $NiCl_2$) and reaction was stopped with tap water. Sections were counterstained with hematoxylin (Leica) for 2 min. After washing and dehydration sections were coverslipped with Neo-Mount. All washes were done with PBS + 0.1% Tween. Images of human tissue samples were taken with a Virtual Slide Microscope VS120 with the Olympus VS-ASW.L100 software (both from Olympus).

2.7. Confocal microscopy and image processing

For fluorescence imaging the Confocal Laser Scanning Microscopes LSM700 and LSM710 from Zeiss were used and gratefully provided by the microscopy core facility of SCI-TReCS (Spinal Cord Injury and Tissue Regeneration Center Salzburg). Images were taken with the ZEN 2011 SP3 or SP7 (black edition) software (all from Zeiss). For qualitative and quantitative analysis images were taken as confocal z-stacks in 20x, 40x or 63x oil magnification and cortical and hippocampal brain regions were assessed. Images were combined to merged maximum intensity projections and edited as well as processed with the ZEN 2012 (blue edition) software (version 1.1.2.0) and Microsoft PowerPoint.

2.8. RNA isolation and gene expression analysis by qPCR

After manual perfusion, animals were decapitated and the brain region of interest was dissected from one brain hemisphere. Brain regions were immediately transferred to RNA later (Sigma) and stored at −80 °C. Tissue was homogenized in 1 mL Trizol (TRI®Reagent; Sigma). For phase separation, 150 μL of 1 bromo-3-chloropropane (Sigma) were added, vortexed and centrifuged (15 min. at 12,000 × *g* at 4 °C). After transferring the aqueous phase into a new tube 1 μL GlycoBlue™ (Invitrogen) and 500 μL 2-Propanol p.A. (Millipore) were added and vortexed. To obtain RNA, samples were centrifuged (10 min. at 12,000 × *g* at 4 °C). The pellet was washed with 1 mL 75% ethanol, dried and re suspended in 30 μL RNase-free water (pre warmed to 55 °C). RNA was stored at −80 °C till further analysis. For analysis of microglia, pro- or anti-inflammatory and phagocytosis related genes and for validation of RNAseq data, cDNA was synthesized using iScript Reverse Transcription Supermix (Bio-Rad) or GoScript Reverse Transcriptase Mix + Random Primers in addition of Oligo(dT) Primer (all from Promega). Quantitative gene expression analyses were performed using TaqMan RT-PCR technology. Technical duplicates containing 10 ng of reverse transcribed RNA were amplified with the GoTAQ Probe qPCR Master Mix (Promega) using a two-step cycling protocol (95 °C for 15 s, 60 °C for 60 s; 40 cycles, Bio-Rad CFX 96 Cycler). The following validated exon-spanning gene expression assays were employed: validated candidate housekeepers were chosen for the present experiment (*PSMD4*, Mm.PT.56.13046188; *G6pdx* Mm.PT.58.13826440; *Ywhaz* Mm.PT.39a.22214831; Heatr3 Mm.PT.56.8463165; all Integrated DNA Technologies). The following primer were used for target gene analysis: *Arg1* (Mm00475988_m1), *H2-Aa* (Mm00439211_m1), *MRC1* (Mm00485148_m1), *Nos2* (Mm00440485_m1), *TNFa* (Mm00443258_m1), *Marco* (Mm00440265_m1, all from Thermofisher); *CCL2* (Mm.PT.56a.42151692), *IL-1ß* (Mm.PT.56a.41616450), *IL-6* (Mm.PT.56a.10005566), *TGFß* (Mm.PT.56a.11254750), *INFg* (Mm.PT.56a.41152792), *CD33* (Mm.PT.58.12829132), *Trem2* (Mm.PT.58.7992121), *TMEM119* (Mm.PT.58.6766267), *AIF1* (Mm.PT.56a.7014816), *Arc* (Mm.PT.58.5865502.g) and *Npas4* (Mm.PT.58.25462031) all from Integrated DNA Technologies. Quantification analyses of inflammation-related genes was performed with qBase Plus (Biogazelle) using geNorm algorithms for multi-reference gene normalization. Data were normalized to WT + PBS gene expression (base line expression) and presented as fold changes. Bars are represented as mean with SD (n = 4–7/group). Quantification of neuronal gene expression (*Arc* and *Npas4*) was performed as follows: mean CT values of the housekeeper genes were subtracted from target gene CT values (ΔCT). The ΔΔCT values were calculated by subtracting the average ΔCT value from WT + PBS mice, that represent baseline gene expression. Fold changes were calculated using $2^{-\Delta\Delta CT}$ formula (Livak and Schmittgen, 2001) for each target gene. Bars are represented as scatter plot with mean and SD (n = 5/group).

2.9. RNAseq analysis and bioinformatics

RNAseq analysis was performed by Qiagen Genomic Services and is shortly outlined as follows: The library preparation was done using TruSeq® Stranded mRNA Sample preparation kit (Illumina inc). The starting material (500 ng) of total RNA was mRNA enriched using the oligo(dT) bead system. The isolated mRNA was subsequently fragmented using enzymatic fragmentation. Then first strand synthesis and second strand synthesis were performed and the double stranded cDNA was purified (AMPure XP, Beckman Coulter). The cDNA was end repaired, 3′ adenylated and Illumina sequencing adaptors ligated onto the fragments ends, and the library was purified (AMPure XP). The mRNA stranded libraries were pre-amplified with PCR and purified (AMPure XP). The libraries size distribution was validated and quality inspected on a Bioanalyzer 2100 or BioAnalyzer 4200 tapeStation (Agilent Technologies). High quality libraries are pooled based in equimolar concentrations based on the Bioanalyzer Smear Analysis tool (Agilent Technologies). The library pool(s) were quantified using qPCR and optimal concentration of the library pool used to generate the clusters on the surface of a flowcell before sequencing on a NextSeq500 instrument (75 cycles) according to the manufacturer instructions (Illumina Inc.).

Quality control of raw sequencing data was conducted using FastQC tool (Andrews, 2010; available online at: http://www.bioinformatics.babraham.ac.uk/projects/fastqc/). Reads were then mapped to the genome (*Mus musculus* genome GRCm38) using bowtie2 (version 2.2.2, Langmead and Salzberg, 2012). Reads that overlap with genes were then counted using HTSEQ tool (version 0.11.2, Anders et al., 2015), -m intersection-nonempty -s no -i gene_id -t exon). Expression values of protein coding genes were first normalized and differential expression analysis between the different groups was conducted using Deseq2 (Love et al., 2014). Genes were considered significantly differentially transcribed with an adjusted p-value < 0.1 (Benjamini & Hochberg multiple testing correction). Enrichment analysis for GO terms and Kegg pathways were conducted using "clusterProfiler" package in R (Yu et al., 2012). Benjamini and Hochberg multiple testing correction was used to adjust raw p-values for multiple testing (adj. p-value < 0.05 were considered significant). In order to summarize and simplify the GO term enrichment results, we used REVIGO (Supek et al., 2011) that relies on semantic similarity measures (Simrel semantic similarity measures was used with default parameters). For hippocampal RNAseq analysis 5 animals per group from WT + PBS, APP-PS1 + PBS and APP-PS1 + anti-CD8 (n = 5/group; mixed gender) were used.

2.10. Blood sera and cytokine analysis:

Total blood was drawn from the heart and let clot at RT. Blood was heated to 37 °C for 1 h and centrifuged full speed for 15 min. Blood sera was taken from the supernatant and stored at −80 °C. To determine mouse blood serum cytokine levels, the U-PLEX Biomarker Group1 (Mouse) Multiplex Assay kit (K15069L-1) from Meso Scale Discovery (MSD) including cytokine standards was used. The U-PLEX assay was performed for pro-inflammatory (IFNγ, IL-1β, IL-6, IL-12p70, TNFα, IP-10, MCP-1) and anti-inflammatory cytokines (IL-4, IL-10) according to the manufacturer's manual. Cytokine levels were measured using the QuickPlex SQ 120 (MSD). Not all cytokines were measurable in our mouse sera samples and together with outliers removed from the analysis. Technical duplicates were averaged and cytokine levels were calculated in pg/mL for each individual animal. Data are depicted as scatter plot showing mean with SD (n = 4–6/group).

2.11. Data analysis

2.11.1. Spleen size analysis

To examine if the antibody treatment might impact the health condition of the animals, we took images of the spleens to quantitatively analyse spleen sizes. We measured length, width and area of the spleens with the image processing software Fiji (ImageJ2) and performed statistical analysis to compare the mean values from the different groups. We took spleen images from 5 to 7 animals per group (n = 5–7).

2.11.2. Quantification of $CD8^+$ T-cells in mouse brains by fluorescence immunohistochemistry (IHC)

For quantification of total $CD8^+$ T-cell numbers in and outside blood vessels, maximum intensity projection images of 3 total sagittal brain sections per animal were taken using a Virtual Slide Microscope VS120 with the Olympus VS-ASW.L100 software (both from Olympus). The number of $CD8^+$ T-cells was counted in the hippocampus, cortex and the corpus callosum using ImageJ software (version 1.51n). Cell numbers per brain region were divided by the respective tissue area and represented as cells/mm^2. Data are shown as scatter plot with mean and SD (n = 4/group).

2.11.3. $CD8^+$ T-cell counts in human post-mortem brain specimen

Human brain tissue images were captured with the Olympus VS120 slide scanner microscope. Images of the total hippocampus section were taken at 20x magnification or 40x magnification for representative images. Quantitative analysis was performed with VS Desktop 2.9 and OlyVia (both Olympus). The total numbers of $CD8^+$ T-cells were manually counted in the hippocampus by using the annotation tool of VS Desktop. The $CD8^+$ T-cells were assigned to be either parenchymal or vascular associated due to their location. Using the polygon function the region of interest, i.e. tissue area, was defined and the tissue area was measured in μm^2. Mean cell numbers were displayed as cells/mm^2 and shown as scatter plot with mean and SD (n = 5–8/group).

2.11.4. Amyloid-beta plaque analysis

Numbers of ThioflavinS$^+$ plaques as well as the average plaque area and volume was measured in APP-PS1 mice using the Imaris image analysis software (Imarisx64 9.1.2, Bitplane). 4 confocal z-stack images at 20x magnification from different brain slices per animal were taken from the cortex and hippocampus and processed with Imaris. The number of plaques per image was calculated and the mean plaque number per animal was calculated. Additionally, the mean plaque area and plaque volume from all individual plaques per image was calculated. The average plaque area and volume was calculated for each individual animal and data are shown as mean with SD (n = 3/group).

2.11.5. $Iba1^+$ cell count

To assess neuroinflammation driven by microglia, $Iba1^+$ cell numbers were analysed on the immunohistological sections. 4 confocal z-stack images at 20x magnification from different brain slices per animal were taken from the cortex and hippocampus and processed with Fiji (ImageJ2) software. Only Dapi and Iba1 double positive cells were manually counted and the mean $Iba1^+$ cell number for each animal was calculated. Data are shown as mean with SD (n = 3/group).

2.12. Statistics

For statistical analysis the GraphPad Prism 7 and 8 software was used. The data were tested for normal distribution using the Shapiro-Wilk or Kolmogorov-Smirnov normality test and were tested for outliers using Grubbs test. Comparing two groups the unpaired Student's *t*-test was used. Welch's correction was performed when variances were significantly different. If more than two groups were compared, a One-way analysis of variance (ANOVA) with Tukey's multiple comparison test was used. For analysis of blood T-cell numbers over time and the analysis of MWM data Two-way RM (repeated measurements) ANOVA with Tukey's multiple comparisons or Bonferroni's multiple comparisons test was performed. For qPCR data Two-way ANOVA with Tukey's multiple comparisions or Fisher's LSD post-test was performed. Correlation analysis was done using Pearson correlation test in GraphPad Prism. The data were depicted as mean with standard deviation (SD) or standard error of the mean (SEM) as indicated in the respective figure legends. P-values of $p < 0.0001$ and $p < 0.001$ were considered extremely significant (**** or ***), $p < 0.01$ very significant (**) and $p < 0.05$ significant (*).

3. Results

3.1. $CD8^+$ T-cells infiltrate the brain in aging and AD pathology

It has recently been shown that $CD8^+$ T-cells are present in the brains of APP-PS1 mice and of AD patients (Ferretti et al., 2016; Gate et al., 2020; Unger et al., 2018a; Unger et al., 2018b). However, exactly when and where these cells appear in the brain, which of course is essential knowledge for any hypothesis regarding a putative role of $CD8^+$ T-cells in the brain, is largely obscure. Here, we analysed the temporal and spatial pattern of $CD8^+$ T-cell infiltration in WT and APP-PS1 transgenic mice ranging from 3 months to 26 months of age in the hippocampus, cortex and corpus callosum. This age range covers an early time point of pre-plaque pathology (3 months old) to already advanced plaque pathology (12–13 months old) to a late stage of

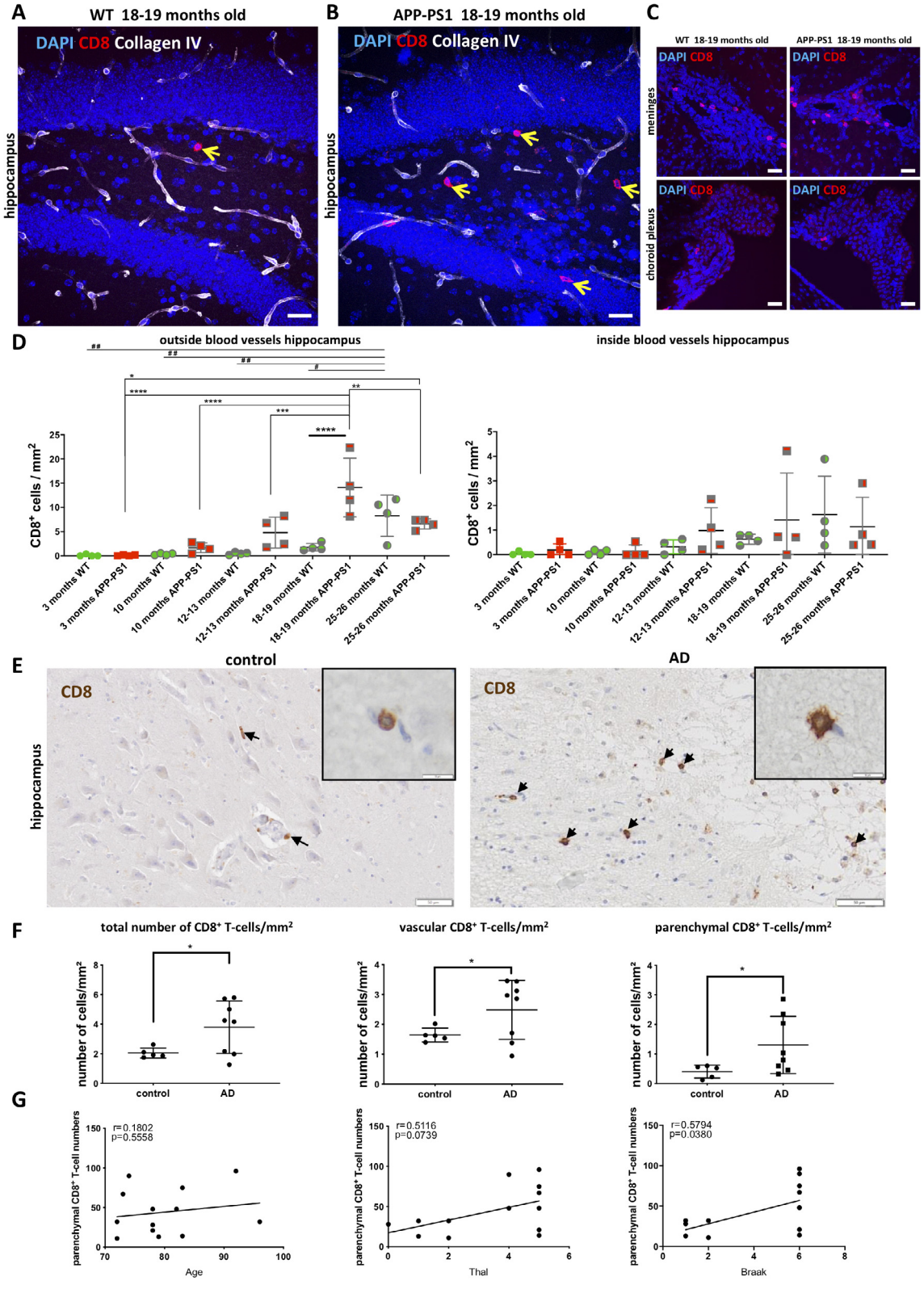

(caption on next page)

pathology (25–26 months old) of the used AD transgenic mouse model (Garcia-Alloza et al., 2006; Hamilton and Holscher, 2012; Unger et al., 2016). We combined CD8$^+$ T-cell staining with Collagen IV, a commonly used blood vessel basement membrane stain (Kniewallner et al., 2018; Kniewallner et al., 2020), which allowed to localize CD8$^+$ T-cells inside or outside of blood vessels, or to be more precise inside or outside of the basement membrane covering the vessels (Fig. 1A, B). Of note, we used only tissue from transcardially perfused animals, which removes the circulating CD8$^+$ T-cells but most likely not the ones that are already attached to the inner vessel wall or about to penetrate into the brain parenchyma.

At the age of 18–19 months CD8$^+$ T-cells could be readily detected

Fig. 1. $CD8^+$ T-cells were identified in the hippocampus brain parenchyma of old WT, transgenic APP-PS1 mice and human AD brain specimen. (A, B) Representative images of Collagen IV^+ (white) blood vessels and $CD8^+$ T-cells (red) in the hippocampus of 18–19 months old WT and APP-PS1 mice. $CD8^+$ T-cells were mainly observed outside of blood vessels (yellow arrow). (C) $CD8^+$ T-cells were also observed in meninges and choroid plexus structures indicating possible routes of entry to the brain parenchyma. (D) Time line analysis of $CD8^+$ T-cell infiltration into the hippocampus: with 12–13 months of age, a trend for increased numbers of $CD8^+$ T-cells outside blood vessels was already observed in the hippocampus of APP-PS1 mice compared to WT animals. In very old animals (18–19 months and 25–26 months) the highest number of brain $CD8^+$ T-cells was detected. The number of $CD8^+$ T-cells inside blood vessels remained unchanged. (E) In human AD hippocampus brain specimen $CD8^+$ T-cells (black arrows) were located at sites of blood vessels, but also directly in the brain parenchyma with increased frequency in AD patients compared to age-matched healthy controls. (F) The total number, the number of vascular and the number of parenchymal $CD8^+$ T-cells per area was significantly increased in human AD hippocampus samples compared to age-matched healthy controls. (G) Parenchymal $CD8^+$ T-cell numbers positively correlate with Braak stage, trend to correlate with Thal but did not correlate with human age. Dapi (A, B, C) and hematoxylin (E) was used as nucleus stain. One-way ANOVA with Tukey's multiple comparisons test (D, n = 4/group) and unpaired Student's *t*-test with Welch's correction was used (F, n = 5–8/group). Pearson correlation was performed in G. Data are shown as scatter plot with mean and SD (D, F). Scale: 25 μm (A, B, C), 50 μm (E) and 10 μm (inserts in E). (For interpretation of the references to colour in this figure legend, the reader is referred to the web version of this article.)

and were significantly increased in the hippocampal brain parenchyma of APP-PS1 compared to WT mice (Fig. 1A, B). The majority of $CD8^+$ T-cells were located within the brain parenchyma distant from blood vessels (Fig. 1A, B, yellow arrows), which was confirmed by the quantitative analysis in the hippocampus (Fig. 1D), the cortex (Supplementary Fig. 1A) and corpus callosum (Supplementary Fig. 1B). Overall, the $CD8^+$ T-cell density was higher in the hippocampus and corpus callosum compared to the cortex (Fig. 1D, Supplementary Fig. 1A, B). While in 3 months old WT and APP-PS1 mouse brains there were hardly any $CD8^+$ T-cells in the hippocampus, cortex and corpus callosum detectable, the APP-PS1 brains from 10 and 12–13 months old mice started to have elevated numbers of $CD8^+$ T-cells compared to age-matched WT mice (Fig. 1D, Supplementary Fig. 1A, B). In WT brains, the number of $CD8^+$ T-cells outside of blood vessels was constantly increasing with the highest numbers of $CD8^+$ T-cells observed in the eldest group (25–26 months of age). In APP-PS1 transgenic mice, the presence of $CD8^+$ T-cells had an earlier onset, was more pronounced and peaked already at the age of 18–19 months old mice compared to WT animals (Fig. 1D, Supplementary Fig. 1A, B). Of note, the number of $CD8^+$ T-cells inside the blood vessels of the perfused animals was only slightly but in most cases not significantly higher in more advanced ages irrespectively of the genotype (Fig. 1D, Supplementary Fig. 1A, B). A possible entry point of $CD8^+$ T-cells into the brain is the meninges and the choroid plexus. Indeed, we frequently observed $CD8^+$ T-cells present in the hippocampal meninges in 18–19 months old WT and APP-PS1 mice, however fewer signals were detected in the choroid plexus of these mice (Fig. 1C). To address if the presence of $CD8^+$ T-cells in the mouse brain is an event specifically related to amyloid plaque pathology, we also stained for $CD8^+$ T-cells in the brains of mouse models for Tau pathology but with no amyloid pathology (Supplementary Fig. 2). However, we barely observed $CD8^+$ T-cells in the hippocampus of these mice and did not observe an association of $CD8^+$ T-cells with pTau positive neurons (Supplementary Fig. 2C-F).

To verify $CD8^+$ T-cell infiltration in human brains and to address if this is even more pronounced in brains from human AD patients, we quantified parenchymal and vascular $CD8^+$ T-cell numbers in post-mortem brain sections from AD patients and old healthy controls (Table 1). In human post-mortem brain specimen, $CD8^+$ T-cells were detected in close association with blood vessels but additionally, and this was even more pronounced in AD samples, $CD8^+$ T-cells were often located intra-parenchymal (Fig. 1E). The total numbers of $CD8^+$ T-cells, the numbers of $CD8^+$ T-cells associated with blood vessels, and the numbers of $CD8^+$ T-cells in the brain parenchyma were higher in AD post-mortem hippocampus sections compared to age-matched healthy controls (Fig. 1F). Remarkably, there is a significant positive correlation of parenchymal $CD8^+$ T-cell numbers with Braak stages, we observed a trend for a positive correlation with Thal but observed no correlation with age in human brain samples within the age range analysed (72 to 96 years of age) (Fig. 1G). We did not detect a correlation of total or vascular $CD8^+$ T-cell numbers in respect to Braak, Thal or age (Supplementary Fig. 1C).

Summarizing, our data demonstrate that $CD8^+$ T-cells infiltrate the hippocampus, cortex and corpus callosum in an age- and pathology dependant manner with the effect starting earlier and being more pronounced in APP-PS1 mice. We confirmed increased numbers of $CD8^+$ T-cells in human AD hippocampus sections and show that $CD8^+$ T-cells directly locate in the brain parenchyma, where their number positively correlates with Braak and Thal staging. Therefore, we hypothesise, that in addition to age classical hallmarks of AD contribute to trigger $CD8^+$ T-cell infiltration into the brain.

3.2. $CD8^+$ T-cells can be successfully ablated from the blood and brain of WT and APP-PS1 mice

To study the functional relevance of $CD8^+$ T-cells and their beneficial or detrimental role in the brain in the context of AD we ablated $CD8^+$ T-cells in WT and APP-PS1 mice. We used WT and APP-PS1 animals with the age of 12 months, a time point where WT animals in contrast to APP-PS1 mice hardly show any $CD8^+$ T-cells in the brain and APP-PS1 mice have already a solid amyloid pathology (Unger et al., 2016; Unger et al., 2018b). We injected the animals *i.p.* with a commercially available anti-CD8a antibody in the dose of 0.8 mg per injection, which had been demonstrated to efficiently ablate the $CD8^+$ T-cells from the organism (Balogh et al., 2018; Laky and Kruisbeek, 2016). For control, we injected animals with either PBS or an isotype control antibody with the same concentration. Treatment lasted for a total of 4 weeks (Fig. 2A). Every week blood was drawn from the *vena saphena* of the mice and $CD8^+$ T-cell ablation was monitored using flow cytometry (Fig. 2B and Supplementary Fig. 3A). Therefore, cells of interest (lymphocytes) were gated for CD3 expression, plotted for CD4 and CD8b and the cell numbers from the frequencies of $CD4^-/CD8^-$, $CD4^+/CD8^-$, $CD4^-/CD8^+$ and $CD4^+/CD8^+$ T-cells were measured in the pool of $CD3^+$ T-cells (Supplementary Fig. 3A). Ablation of $CD8^+$ T-cells was constant over the weeks of treatment. In last week of treatment, because of behavioural testing during this period, blood was taken only via cardiac puncture before transcardial perfusion of the animals. $CD4^-/CD8^+$ T-cells were successfully eliminated from the blood of WT and APP-PS1 animals receiving anti-CD8 antibody treatment (Fig. 2B, C). Interestingly, while in the pool of $CD3^+$ cells the numbers of $CD4^-/CD8^+$ T-cells was drastically reduced, the numbers of $CD4^+/CD8^-$ T-cells and $CD4^-/CD8^-$ T-cells was significantly increased in the blood of WT and APP-PS1 receiving the anti-CD8 antibody treatment (Fig. 2D, E). Additionally, we analysed the overall percentage of $CD3^+$ T-cells in the blood of WT and APP-PS1 mice with treatment over time and observed significantly reduced $CD3^+$ T-cell percentages in the first week of anti-CD8 antibody treatment (Supplementary Fig. 3C). Overall, there was a trend for reduced total $CD3^+$ T-cell frequencies in the blood. This indicates a compensatory mechanism in the organism in terms of a reduction in overall $CD3^+$ T-cell numbers and a shift in the pool of $CD3^+$ T-cells towards highly reduced $CD4^-/CD8^+$ but increased $CD4^+/CD8^-$ and $CD4^-/CD8^-$ T-cells. The treatment did not cause any adverse events as a loss of body weight (data not shown) nor did we observe any morphological

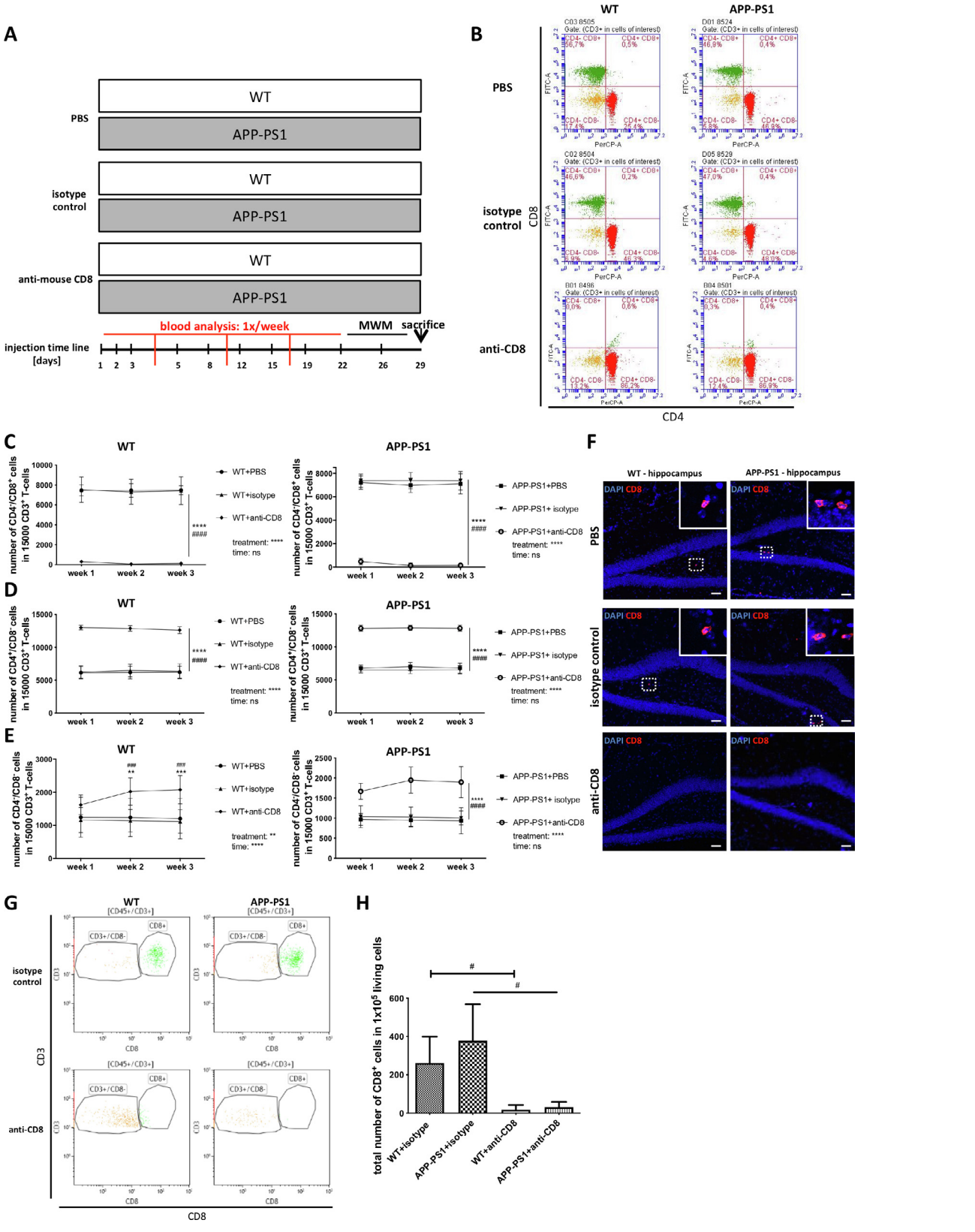

(caption on next page)

alterations in size of spleens (Supplementary Fig. 3D-G). Animals did not show increased signs of sickness due to anti-CD8 antibody treatment. We also investigated the number of $CD4^+/CD8^-$ and $CD4^-/CD8^+$ T-cells in WT and APP-PS1 mice receiving only PBS and calculated the blood CD4:CD8 ratio over the time (Supplementary Fig. 3B). We did not observe altered baseline levels of this T-cell populations in the blood of APP-PS1 animals compared to WT controls, at least not at this age.

To assess if the systemic anti-CD8 antibody treatment also ablated $CD8^+$ T-cells in secondary lymphoid organs we histologically stained

Fig. 2. In vivo CD8$^+$ T-cell ablation experiment and successful elimination of CD8$^+$ T-cells from the blood and the brain of WT and APP-PS1 animals. To analyze the role of CD8$^+$ T-cells in AD pathology, CD8$^+$ T-cells were ablated using an anti-CD8 antibody treatment. (A) Experimental set up: WT and APP-PS1 mice were treated for a total of 4 weeks with either PBS, isotype control or anti-CD8 antibody. Animals were injected i.p. for 3 consecutive days and on day 5, followed by 2 injections per week for a total of 10 injections á 0.8 mg antibody. Once per week blood was drawn from vena saphena to monitor CD8$^+$ T-cell ablation in PBMCs. In the last week of treatment MWM behavior test was performed. (B) Representative flow cytometry dot plots showing ablation of the CD8$^+$ T-cell pool in the blood of anti-CD8 treated mice (green population). Cells of interest were gated for CD3 and further gated for CD4 or CD8b to discriminate single or double positive cell populations. (C) Quantitative analysis of CD4$^-$/CD8$^+$ T-cell frequencies from the blood showed significantly reduced cell numbers over 3 weeks in WT and APP-PS1 mice receiving the anti-CD8 antibody treatment. (D) Interestingly, in the pool of analyzed CD3$^+$ T-cells the CD4$^+$/CD8$^-$ and CD4$^-$/CD8$^-$ cell numbers (E) were elevated in the anti-CD8 treated animals. (F) Histological staining for CD8$^+$ T-cells (red) in the hippocampus illustrating successful ablation of CD8$^+$ T-cells with anti-CD8 treatment in WT and APP-PS1 animals. (G) Representative flow cytometry dot plots of CD3$^+$/CD8$^+$ T-cells (green) isolated from total brain hemispheres of WT and APP-PS1 animals receiving isotype control or anti-CD8 antibody. Single-living CD45$^+$/CD3$^+$ cells were gated for CD4 or CD8 expression. (H) Quantitative analysis of brain isolated CD3$^+$/CD8$^+$ T-cells revealed significantly decreased cell numbers in anti-CD8 treated mice compared to isotype controls. Two-way RM ANOVA with Tukey's multiple comparisons test (C: WT treatment: $F(2, 24) = 210.3$, WT time: $F(2, 48) = 2.258$, APP-PS1 treatment: $F(2, 24) = 592.6$, APP-PS1 time: $F(2, 48) = 2.975$; D: WT treatment: $F(2, 24) = 172.3$, WT time: $F(2, 48) = 1.287$, APP-PS1 treatment: $F(2, 24) = 533.2$, APP-PS1 time: $F(2, 48) = 0.6492$; E: WT treatment: $F(2, 24) = 7.324$, WT time: $F(2, 48) = 16.97$, APP-PS1 treatment: $F(2, 24) = 48.09$, APP-PS1 time: $F(2, 48) = 1.361$; n = 8–10/group) and One-way ANOVA with Tukey's multiple comparisons test and unpaired Student's *t*-test comparing WT + isotype vs. WT + anti-CD8 mice (H, n = 3/group) was performed. Data are shown as mean with SD (C, D, E, H). * indicates significance comparing anti-CD8 vs. PBS, # indicates significance comparing anti-CD8 vs. isotype control. Dapi was used as nucleus stain. Scale: 50 μm (F). (For interpretation of the references to colour in this figure legend, the reader is referred to the web version of this article.)

for CD8 in the spleen and demonstrated successful elimination of CD8$^+$ T-cells in WT and APP-PS1 spleens (Supplementary Fig. 3H). Additionally, after 4 weeks of treatment we stained for CD8$^+$ T-cells in the hippocampus (Fig. 2F) and performed flow cytometry analysis on brain isolated T-cells (Fig. 2G). There were no CD8$^+$ T-cells detected in the hippocampus of anti-CD8 antibody treated mice and the number of brain isolated CD8$^+$ T-cells was highly reduced in anti-CD8 antibody treated animals compared to isotype control antibody receiving mice (Fig. 2H). Taken together these data demonstrate successful ablation of CD8$^+$ T-cells from the blood, spleen and the brain of WT and APP-PS1 mice and that the ablation was well tolerated by the animals.

3.3. CD8$^+$ T-cell ablation did not restore learning deficits in 12–13 months old APP-PS1 mice and had no impact on amyloid pathology

First we analysed spatial learning and memory in APP-PS1 mice and addressed the question if anti-CD8 antibody treatment altered cognition in these animals (Fig. 3). We performed the MWM test in the last week of treatment, where the animals had to find a water-submerged hidden platform. We analysed the overall search and learning behaviour over time. APP-PS1 mice compared to WT mice had significantly higher swim speeds (Fig. 3B), a significantly altered searching behaviour in terms of increased time spent in the arena wall zone also known as thigmotaxis (Fig. 3F) and we observed that APP-PS1 mice moved with significantly higher distances until they reached the platform (Fig. 3J). Of note memory of the original platform position was unchanged in APP-PS1 mice compared to WT mice (data not shown). Altogether, APP-PS1 mice had a highly altered search and learning behaviour in the MWM test. The anti-CD8 antibody treatment and the resulting ablation of CD8$^+$ T-cells did not restore these learning deficits in APP-PS1 mice (Fig. 3D, H, L). There were no adverse effects of treatment on the above-analysed parameters in WT mice (Fig. 3C, G, K).

One of the main hallmarks of AD pathology is the formation of amyloid-beta plaques. In a next approach we therefore analysed amyloid plaque pathology after CD8$^+$ T-cell depletion in the mostly affected brain regions as the cortex and hippocampus from APP-PS1 mice (Fig. 4A). We did not observe any changes in overall plaque numbers (Fig. 4B) or plaque morphology, i.e. individual plaque area or volume (Fig. 4C, D). We conclude from our data that amyloid plaque pathology is not altered after ablation of CD8$^+$ T-cells at this time point of disease progression.

3.4. CD8$^+$ T-cell ablation increased Iba1$^+$ cell numbers in the hippocampus

In a next approach we analyzed the effects of CD8$^+$ T-cell ablation on peripheral inflammation and neuroinflammation, especially on microglia cells (Fig. 5). For that, we first measured blood sera cytokine levels for pro-inflammatory cytokines as IL-6, IP-10, IFNy, TNFa and MCP-1 as well as the anti-inflammatory cytokine IL-10 (Fig. 5A). APP-PS1 mice did not have a different peripheral cytokine profile compared to WT mice, and moreover, the ablation of CD8$^+$ T-cells did not result in altered cytokine levels in neither WT nor APP-PS1 animals (Fig. 5A). To investigate the overall immune signature in the brain, we performed gene expression analysis of the cortex and hippocampus for microglia (*Aif1*, *Tmem119*), pro-inflammatory (*Ccl2*, *H2-Aa*, *IFNg*, *IL-1beta*, *IL6*, *Marco*, *Nos2*, *TNFa*), anti-inflammatory (*Arg1*, *MRC1*, *TGFbeta*) and phagocytosis (*Trem2*, *CD33*) related genes (Fig. 5B, C). In APP-PS1 cortex and/or hippocampus expression of microglia genes and of *H2-Aa*, *IL-1beta* and *Trem2* was higher compared to WT mice (Fig. 5B, C). Upon CD8$^+$ T-cell ablation expression of the above-investigated genes

Table 1
Clinical and neuropathological data of human post-mortem hippocampus specimen used for the analysis: Total numbers of CD8$^+$ T-cells, vascular CD8$^+$ T-cells and parenchymal CD8$^+$ T-cells were quantified in AD and age-matched healthy control samples.

Sample ID	Age	Gender	Braak	Thal	CERAD	NIA-R	Diagnosis	Total CD8$^+$ T-cell numbers	Vascular	Parenchymal
52_93T	96	F	1	1	0	Low	Control	118	86	32
64_96	72	F	2	2	0	Low	Control	140	108	32
98_98	78	F	1	0	0	Not	Control	105	77	28
102_5	72	M	2	2	0	Low	Control	154	143	11
201_93U	79	F	1	1	0	Low	Control	111	98	13
11_04	73	F	6	5	3	High	AD	223	156	67
57_92	74	M	6	4	3	High	AD	222	132	90
67_98	83	F	6	5	3	High	AD	150	75	75
74_97R	78	F	6	5	3	High	AD	100	79	21
77_97x	82	F	6	5	3	High	AD	257	209	48
92_00L	92	F	6	5	2	High	AD	236	140	96
151_92S	83	F	6	5	3	High	AD	55	41	14
197_96	78	M	6	4	3	High	AD	192	144	48

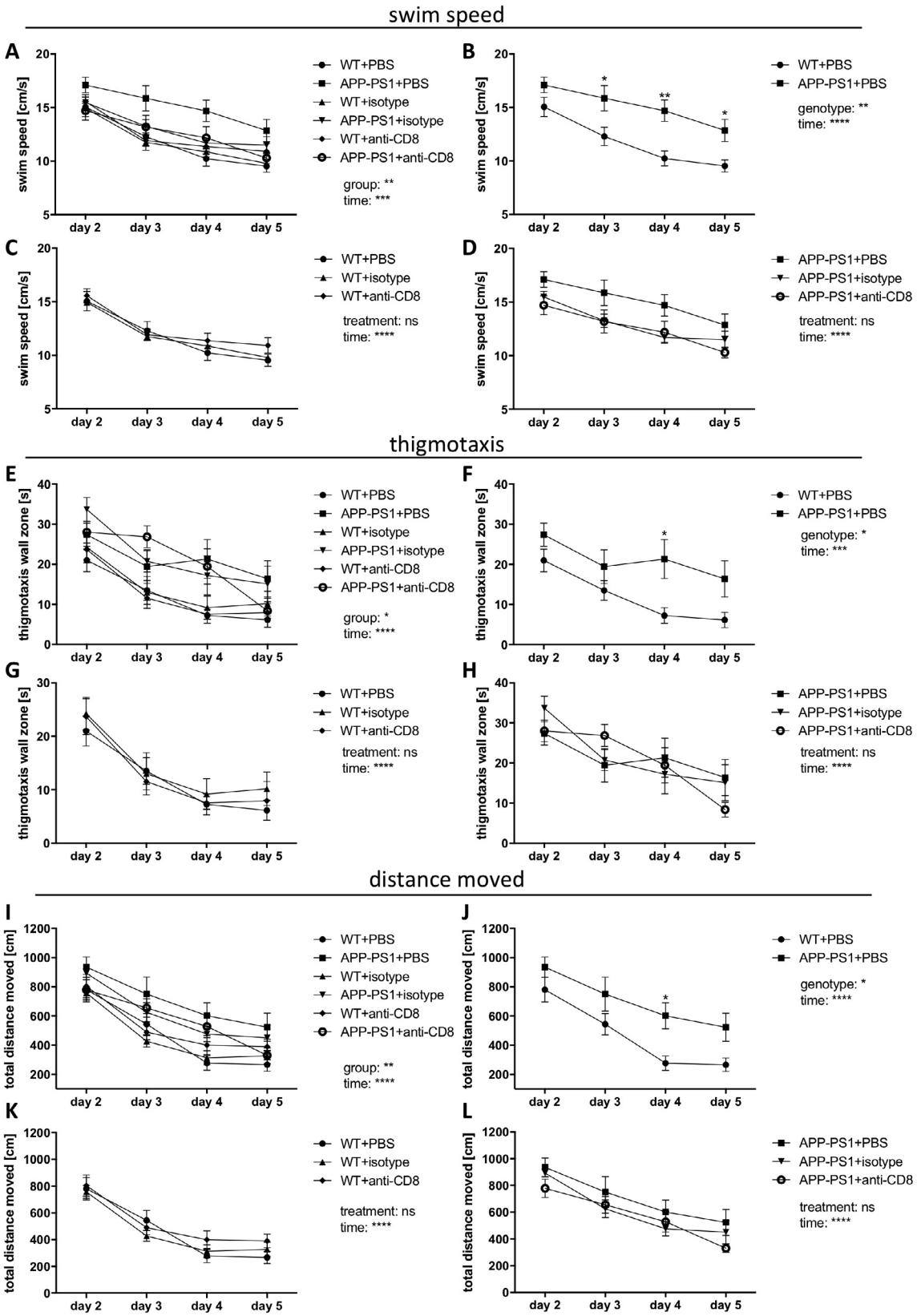

(caption on next page)

was not altered in WT or APP-PS1 mice, except for a downregulation of the phagocytosis-related *Trem2* gene in the cortex of APP-PS1 + anti-CD8 mice (Fig. 5B). This, together with our previous finding that $CD8^+$ T-cells often are in close contact with microglia in APP-PS1 brains (Unger et al., 2018b), induced us to analyze microglia more in detail. First we quantified brain-isolated microglia ($CD11b^+/CD45^{low}$) and macrophages ($CD11b^+/CD45^{high}$) using flow cytometry (Fig. 5D), as this is a widely used method to differentiate between microglia and

Fig. 3. Spatial learning and behaviour assessment using the Morris Water Maze (MWM) test: Swim speed, thigmotaxis behaviour and the distance the animals moved to reach the water submerged hidden platform was analysed. (A-D) APP-PS1 animals had an overall higher swim speed compared to WT mice. Anti-CD8 treatment did not alter the swim speed in WT or APP-PS1 mice. (E-H) Thigmotaxis (i.e. wall hugging) behaviour was analysed by measuring the time animals spent in the arena wall zone. APP-PS1 mice spent significantly increased time at the wall zone compared to WT mice. Anti-CD8 treatment did not alter thigmotaxis behaviour in APP-PS1 mice. (I-L) APP-PS1 mice significantly moved with higher distances compared to WT mice to reach the platform. Anti-CD8 antibody treatment had no impact on the distance moved of WT or APP-PS1 mice. Data are shown as mean with SEM (A-L). Two-way RM ANOVA with Tukey's multiple comparisons test (A: group: $F(5, 48) = 3.746$, time: $F(3, 144) = 93.79$; C: treatment: $F(2, 24) = 0.6018$, time: $F(3, 72) = 53.76$; D: treatment: $F(2, 24) = 3.121$, time: $F(3, 72) = 41.76$; E: group: $F(5, 48) = 3.408$, time: $F(3, 144) = 42.26$; G: treatment: $F(2, 24) = 0.357$, time: $F(3, 72) = 24.82$; H: treatment: $F(2, 24) = 0.03075$, time: $F(3, 72) = 19.65$; I: group: $F(5, 48) = 4.088$, time: $F(3, 144) = 75.14$; K: treatment: $F(2, 24) = 1.07$, time: $F(3, 72) = 42.86$; L: treatment: $F(2, 24) = 1.392$, time: $F(3, 72) = 33.85$) or Bonferroni's multiple comparisons test (B: genotype: $F(1, 16) = 9.103$, time: $F(3, 48) = 35.24$; F: genotype: $F(1, 16) = 7.387$, time: $F(3, 48) = 7.872$; J: genotype: $F(1, 16) = 7.724$, time: $F(3, 48) = 22.53$) was used (n = 8–10/group).

macrophages (Becher and Antel, 1996; Bennett et al., 2016; Ford et al., 1995; Korin et al., 2017). The number of $CD11b^+/CD45^{low}$ and of $CD11b^+/CD45^{high}$ cells isolated from brains of APP-PS1 mice was higher compared to the ones from WT mice (Fig. 5E, F). The anti-CD8 treatment slightly elevated the fraction of $CD11b^+/CD45^{high}$ cells (presumably macrophages) in the APP-PS1 mice (Fig. 5F). We analyzed this in more detail using immunohistochemistry and quantified the number of $Iba1^+$ cells in the cortex and hippocampus (Fig. 5G, H, I). Indeed, we confirmed our finding and observed significantly higher numbers of $Iba1^+$ cells upon $CD8^+$ T-cell ablation in the hippocampus of APP-PS1 mice but not in WT mice (Fig. 5I).

We conclude from our data, that the anti-CD8 antibody treatment and the resulting ablation of $CD8^+$ T-cells had no impact on peripheral and central cytokine expression. Nevertheless, while it increased the number of $Iba1^+$ cells in the hippocampus of APP-PS1 mice it reduced the expression of the phagocytosis-related *Trem2* gene.

3.5. Hippocampal RNAseq revealed significantly altered neuronal- and synapse-related gene expression in APP-PS1 mouse brains lacking $CD8^+$ T-cells

To unravel the function of brain $CD8^+$ T-cells and possible alterations in the CNS upon their ablation, we isolated total RNA from the hippocampus of WT + PBS, APP-PS1 + PBS and APP-PS1 + anti-CD8 mice and performed RNAseq analysis. First, we investigated for differences between APP-PS1 and WT mice. We identified 457 genes to be

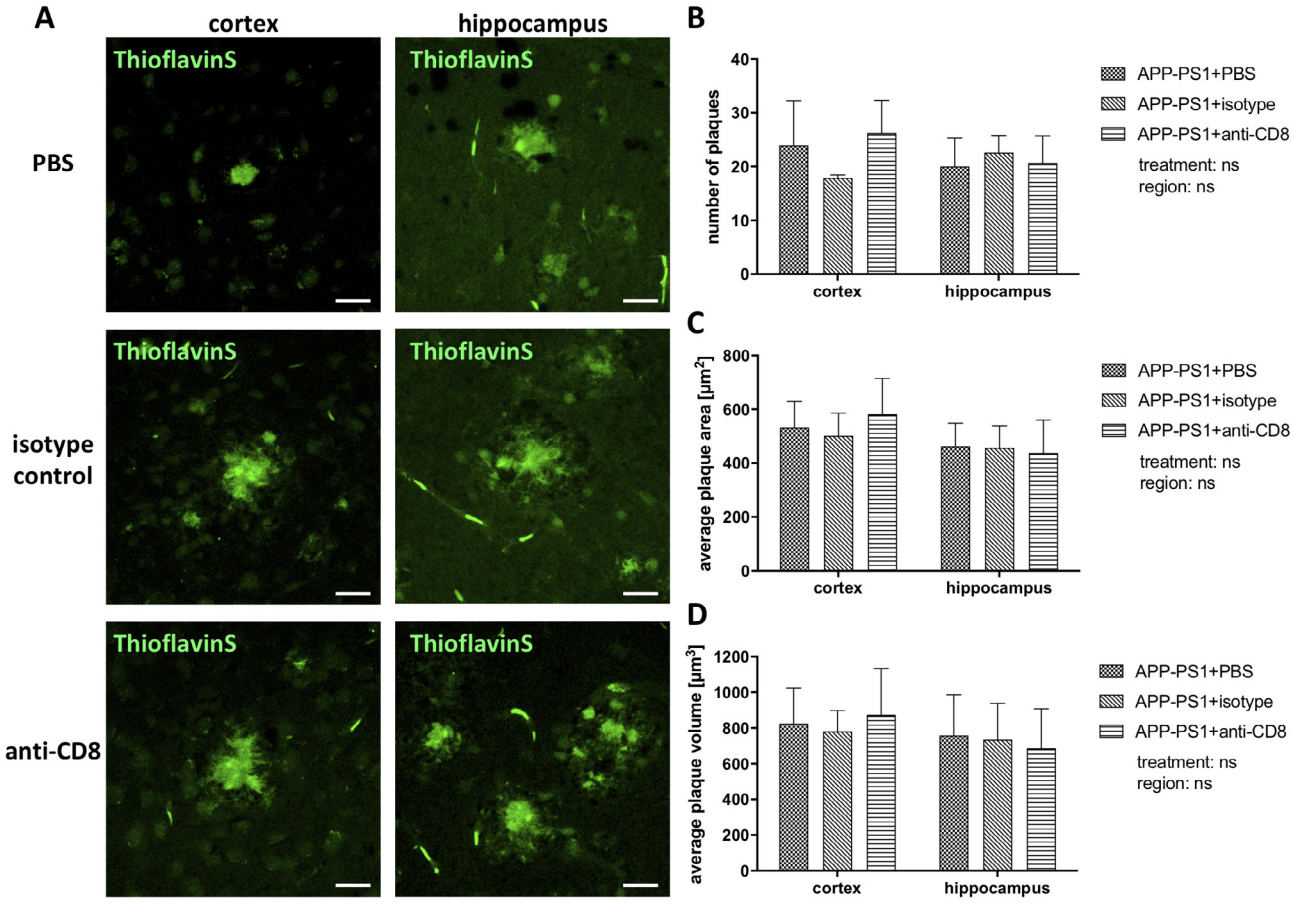

Fig. 4. Analysis of amyloid pathology in cortical and hippocampal brain regions: (A) Representative images of ThioflavinS stained amyloid plaques (green) in the cortex and hippocampus of APP-PS1 mice treated with PBS, isotype control or anti-CD8 antibody. (B) The number of $ThioflavinS^+$ plaques was quantified and there was no difference in the number of plaques upon anti-CD8 antibody treatment in the cortex or hippocampus. (C) Analysis of the individual average plaque area revealed no difference upon anti-CD8 treatment. (D) Additionally, average plaque volume was unchanged in APP-PS1 + anti-CD8 animals compared to respective controls. ThioflavinS was used to stain amyloid plaques. Two-way ANOVA with Tukey's multiple comparisons test was used (B: treatment: $F(2, 12) = 0.5454$, region: $F(1, 12) = 0.4121$; C: treatment: $F(2, 12) = 0.1332$, region: $F(1, 12) = 3.127$; D: treatment: $F(2, 12) = 0.03987$, region: $F(1, 12) = 1.035$; n = 3/group). Data are shown as mean with SD. Scale: 20 µm (A). (For interpretation of the references to colour in this figure legend, the reader is referred to the web version of this article.)

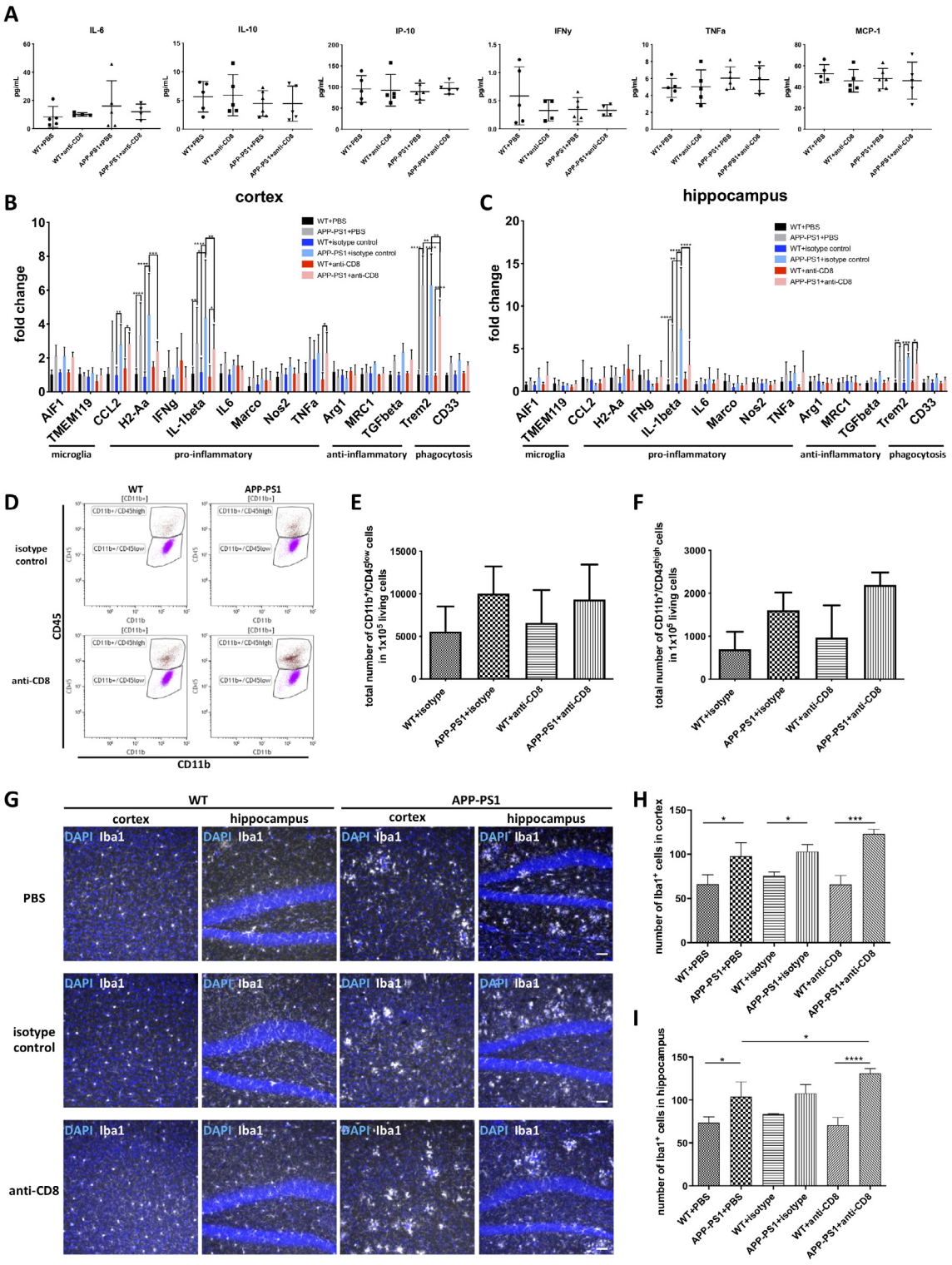

Fig. 5. Analysis of peripheral immune alterations and brain neuroinflammation upon anti-CD8 treatment: (A) Mouse blood sera was analysed for various cytokines (IL-6, IL-10, IP-10, IFNy, TNFa, MCP-1). Cytokine levels were not different in APP-PS1 compared to WT mice and anti-CD8 antibody treatment did not change peripheral cytokine levels in the sera of WT or APP-PS1 mice. (B, C) Gene expression analysis of microglia (*Aif1*, *Tmem119*), pro-inflammatory (*Ccl2*, *H2-Aa*, *Ifng*, *Il-1beta*, *Il6*, *Marco*, *Nos2*, *Tnfa*), anti-inflammatory (*Arg1*, *Mrc1*, *Tgfbeta*) and phagocytosis (*Trem2*, *CD33*) related genes in the cortex and hippocampus upon anti-CD8 antibody treatment. (D) Representative flow cytometry dot blots of brain resident microglia ($CD11b^+/CD45^{low}$) and macrophage ($CD11b^+/CD45^{high}$) cell populations. (E) The number of brain $CD11b^+/CD45^{low}$ microglia trend to be increased in APP-PS1 mice compared to WT. (F) Similarly, the number of brain $CD11b^+/CD45^{high}$ macrophages trend to be increased in APP-PS1 compared to WT mice and also showed a trend to be elevated in APP-PS1 + anti-CD8 animals compared to respective isotype controls. (G) Representative immunohistological images of $Iba1^+$ cells in the cortex and hippocampus. (H) Quantification of $Iba1^+$ cells in the cortex revealed significantly increased numbers of $Iba1^+$ cells in APP-PS1 compared to WT mice. (I) In the hippocampus, $Iba1^+$ cell numbers were significantly increased in APP-PS1 compared to WT mice and surprisingly $Iba1^+$ cell numbers were significantly increased in APP-PS1 mice receiving anti-CD8 antibody treatment compared to respective PBS controls. One-way ANOVA with Tukey's multiple comparisons test (A, n = 4–6/group; E, F, H, I, n = 3/group) and Two-way ANOVA with Tukey's multiple comparisons test (B: gene: F (14, 437) = 23.19, group: F (5, 437) = 44.92; C: gene: F (14, 433) = 8.331, group: F (5, 433) = 8.412; n = 4–7/group) were used. Data are shown as mean with SD. Dapi was used as nucleus stain (G). Scale: 50 μm (G).

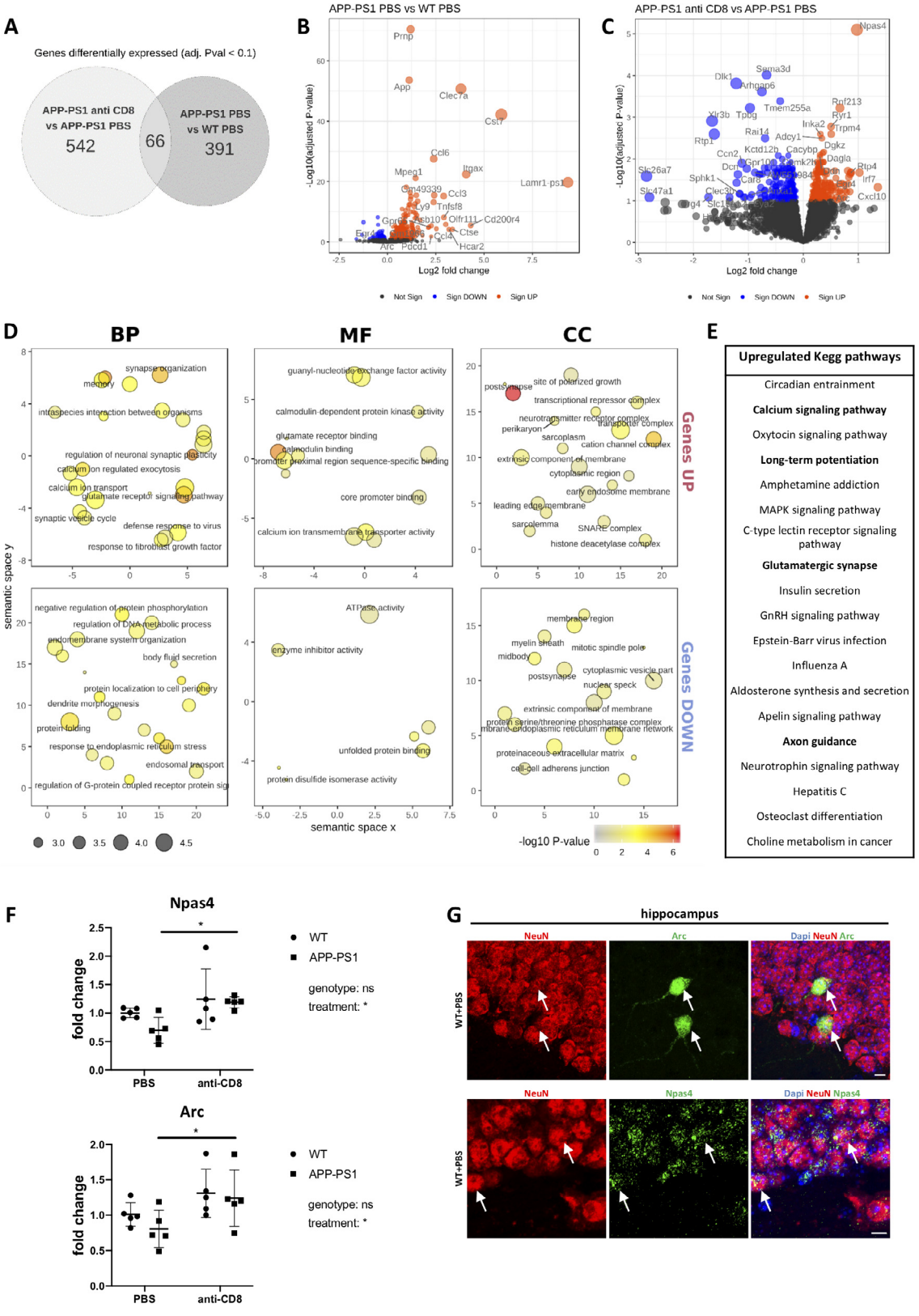

(caption on next page)

significantly differentially expressed in APP-PS1 versus WT hippocampus (Fig. 6A). In general, the hippocampus of APP-PS1 mice revealed a high number of up-regulated genes compared to WT mice (Fig. 6B; a full list of the significantly up- and down-regulated genes including a phenotype description is listed in Supplementary File 1).

Gene ontology (GO) enrichment analysis on the significantly regulated genes in the hippocampus of APP-PS1 mice revealed gene sets for biological processes to be highly enriched including *positive regulation of cytokine production*, *antigen processing and presentation of peptide antigen*, *myeloid leukocyte activation*, *phagocytosis* but also *activation of immune*

Fig. 6. RNAseq analysis of hippocampal transcriptome from WT, APP-PS1 and APP-PS1 mice lacking CD8$^+$ T-cells. (A) Venn diagram showing the overlap of significantly differentially expressed genes (adjusted p-value < 0.1) in APP-PS1 + PBS versus WT + PBS and APP-PS1 + anti-CD8 versus APP-PS1 + PBS animals. (B) Volcano plot of significantly differentially expressed genes and their respective fold changes in APP-PS1 + PBS versus WT + PBS showing a higher number of up-regulated genes in APP-PS1 mice. (C) Volcano plot of significantly differentially expressed genes and their respective fold changes in APP-PS1 + anti-CD8 versus APP-PS1 + PBS mice. Top up-regulated genes include *Npas4* and *CXCL10*. (D) Semantic GO term enrichment analysis of up-regulated and down-regulated hippocampal genes for biological processes (BP), molecular function (MF) and cellular components (CC) in APP-PS1 mice lacking CD8$^+$ T-cells. (E) Up-regulated Kegg pathways in the hippocampus of APP-PS1 + anti-CD8 mice (sorted after adj. p-values) including *calcium signaling*, *long-term potentiation*, *glutamatergic synapse* and *axon guidance* pathways (bold). (F) Validation of *Npas4* and *Arc* gene expression in the hippocampus using qPCR. *Arc* and *Npas4* gene expression was up-regulated in APP-PS1 mice receiving the anti-CD8 antibody treatment compared to respective PBS control. (G) Immunohistochemistry staining for Arc and Npas4 in the hippocampus of WT mice revealed high expression of Arc and Npas4 protein (green) in mature neurons (NeuN, red) in the granular cell layer of the dentate gyrus (arrow). Genes with an adjusted p-value below p < 0.10 were considered significantly differentially expressed (n = 5/group, A-C). Two-way ANOVA with Fisher's LSD post-test was performed and data are shown as scatter plot with mean and SD (F: Npas4: treatment: F (1, 16) = 7.695, genotype: F (1, 16) = 1.831; Arc: treatment: F (1, 16) = 7.218, genotype: F (1, 16) = 1.026; n = 5/group). Dapi was used as nucleus stain. Scale: 5 μm (G). (For interpretation of the references to colour in this figure legend, the reader is referred to the web version of this article.)

response and *T cell activation*, just to name a few (Supplementary Fig. 4A and Supplementary File 1). Enriched GO terms for cellular components included the *phagocytic vesicles/lytic vacuole*, *receptor complex*, *membrane raft* and the *inflammasome complex* (Supplementary Fig. 4A and Supplementary File 1). Down-regulated biological processes in the hippocampus of APP-PS1 mice included *regulation of synaptic plasticity*, *exploration behaviour*, *cellular response to calcium ion*, *chemical synapse transmission postsynaptic*, *learning*, *cognition* and *regulation of synapse structure or activity* (Supplementary Fig. 4A and Supplementary File 1). Under-represented GO terms for cellular components included *postsynapse*, *neuron spine* and *excitatory synapses* (Supplementary Fig. 4A and Supplementary File 1). These data indicate highly up-regulated gene expression for inflammatory processes in the hippocampus of APP-PS1 mice. Additionally or even as consequence, neuronal- and synapse-related gene expression was severely reduced in the hippocampus of APP-PS1 mice compared to WT animals. A full list of regulated genes, GO enrichment analysis and Kegg pathways is shown in Supplementary Fig. 4A, B and Supplementary File 1.

The CD8$^+$ T-cell ablation in the APP-PS1 mice regulated 608 genes in comparison to APP-PS1 PBS-treated control animals (Fig. 6A). 66 genes were shared differentially expressed, i.e. they were differentially expressed in APP-PS1 + PBS mice and regulated by the anti-CD8 antibody treatment (Fig. 6A, intersection of circles). Taking into account the low numbers of hippocampus infiltrating CD8$^+$ T-cells in APP-PS1 mice of 12–13 months of age (see Fig. 1D), fold changes in gene expression after anti-CD8 antibody treatment were low and the majority of all significantly differentially expressed genes were located in a range of −1 to +1 log2 fold changes in APP-PS1 + anti-CD8 mice (Fig. 6C). In Table 2 the top 10 most significantly differentially expressed genes in APP-PS1 + anti-CD8 mice according to their adjusted p-values are listed including the top up-regulated gene *Npas4* and top down-regulated gene *Sema3d* (Table 2). Most interestingly the *Npas4* gene was also one of the up-regulated genes with the highest fold change together with *Cxcl10*, *Irf7*, *Rtp4* and *Arc* (see Table 3, up-regulated genes with highest fold changes). Top down-regulated genes according to their fold changes upon CD8$^+$ T-cell ablation were genes of the solute carrier family as *Slc26a7* and *Slc47a1* (Table 4, down-regulated genes with highest fold changes). A list of all significantly differentially expressed genes in the hippocampus of APP-PS1 + anti-CD8 mice is listed in Supplementary File 2.

Table 2
List of Top 10 most significantly differentially expressed genes in APP-PS1 + anti-CD8 mice compared to APP-PS1 + PBS mice sorted after the adjusted p-values (adj. p < 0.1).

Gene	Description	Fold change (log2)	Adj. p-value (< 0.1)
Npas4	neuronal PAS domain protein 4	0.98	7.99E-06
Sema3d	sema domain, immunoglobulin domain (Ig), short basic domain, secreted, (semaphorin) 3D	−0.67	9.70E-05
Dlk1	delta like non-canonical Notch ligand 1	−1.22	1.54E-04
Arhgap6	Rho GTPase activating protein 6	−0.75	2.43E-04
Tmem255a	transmembrane protein 255A	−0.42	4.13E-04
Tpbg	trophoblast glycoprotein	−0.97	6.01E-04
Rnf213	ring finger protein 213	0.67	6.01E-04
Xlr3b	X-linked lymphocyte-regulated 3B	−1.66	1.23E-03
Ryr1	ryanodine receptor 1, skeletal muscle	0.5	1.69E-03
Rtp1	receptor transporter protein 1	−1.62	2.53E-03

Performing gene ontology enrichment analysis on all significantly up-regulated gene sets in APP-PS1 + anti-CD8 mice revealed over-representation of GO terms for biological processes as *memory, synapse organization, regulation of neuronal synaptic plasticity*, *glutamate receptor signaling pathway* and *synaptic vesicle cycle* (Fig. 6D and Supplementary File 2). Genes related to cellular components included the *postsynapse*, *cation channel complex*, *transporter complex*, and the *SNARE complex* (Fig. 6D and Supplementary File 2). Enriched molecular functions were *glutamate receptor binding*, *calmodulin binding*, *guanyl-nucleotide exchange factor activity* and *calcium ion transmembrane transporter activity* (Fig. 6D and Supplementary File 2). Down-regulated biological processes included *protein folding* and *response to endoplasmic reticulum stress* (Fig. 6D and Supplementary File 2). Cellular components that were under-represented involved the *membrane region*, the *midbody* and the *endoplasmic reticulum membrane network* (Fig. 6D and Supplementary File 2). In summary, these data indicate that in the hippocampus of APP-PS1 mice lacking CD8$^+$ T-cells, neuronal- and synapse-related gene expression is highly increased.

Additionally to the gene ontology enrichment assessment, we performed Kegg pathway analysis on the significantly up-regulated genes of the hippocampus from APP-PS1 mice lacking CD8$^+$ T-cells. Most interestingly, significantly up-regulated pathways included the *calcium signaling pathway*, *long-term potentiation*, *glutamatergic synapse* and *axon guidance* as well as pathways related to *Epstein-Barr virus infection* and *Influenza A* (Fig. 6E). Detailed analysis on all up-regulated Kegg pathways and pathway-associated genes are listed in Table 5. A full list of all regulated genes, GO enrichment analysis and the Kegg pathways is shown in Supplementary File 2. The herein performed Kegg pathway analysis let highly suggest that a lack of CD8$^+$ T-cells in the hippocampus of APP-PS1 mice alters calcium signaling and synapse plasticity in the brain.

According to our data from the hippocampal RNAseq analysis, we conclude that CD8$^+$ T-cell ablation in APP-PS1 mice up-regulated neuronal- and synapse-related gene expression. We validated genes of the RNAseq data by performing qPCR of *Npas4* and *Arc* gene expression, two top up-regulated genes that belong to the family of immediate early genes (IEGs). Indeed, our qPCR results confirmed the RNAseq data and showed an increase in gene expression for *Npas4* and *Arc* in APP-PS1 + anti-CD8 mice compared to APP-PS1 + PBS controls (Fig. 6F). Additionally, *Npas4* gene expression trend to be decreased in the hippocampus of APP-PS1 + PBS mice compared to WT + PBS mice, which was also observed in the RNAseq (Fig. 6F and Supplementary File 1). Since we performed bulk RNAseq from the total hippocampus we

Table 3
List of Top 10 up-regulated genes in APP-PS1 + anti-CD8 mice compared to APP-PS1 + PBS mice sorted after their fold changes.

Gene	Description	Fold change (log2)	Adj. p-value (< 0.1)
Cxcl10	chemokine (C-X-C motif) ligand 10	1.36	4.76E-02
Irf7	interferon regulatory factor 7	1.02	2.12E-02
Npas4	neuronal PAS domain protein 4	0.98	7.99E-06
Rtp4	receptor transporter protein 4	0.87	2.12E-02
1700016P03Rik	RIKEN cDNA 1700016P03 gene	0.86	2.12E-02
Egr4	early growth response 4	0.85	2.34E-02
Arc	activity regulated cytoskeletal-associated protein	0.85	6.05E-02
Isg15	ISG15 ubiquitin-like modifier	0.83	2.72E-02
Pla2g4e	phospholipase A2, group IVE	0.82	4.00E-02
Gck	glucokinase	0.81	1.91E-02

Table 4
List of Top 10 down-regulated genes in APP-PS1 + anti-CD8 mice compared to APP-PS1 + PBS mice sorted after their fold changes.

Gene	Description	Fold change (log2)	Adj. p-value (< 0.1)
Slc26a7	solute carrier family 26, member 7	−2.85	2.58E-02
Slc47a1	solute carrier family 47, member 1	−2.8	8.23E-02
Prg4	proteoglycan 4 (megakaryocyte stimulating factor, articular superficial zone protein)	−1.72	8.23E-02
Xlr3b	X-linked lymphocyte-regulated 3B	−1.66	1.23E-03
Rtp1	receptor transporter protein 1	−1.62	2.53E-03
Hif3a	hypoxia inducible factor 3, alpha subunit	−1.34	8.23E-02
Dlk1	delta like non-canonical Notch ligand 1	−1.22	1.54E-04
Car8	carbonic anhydrase 8	−1.21	3.71E-02
Dcn	decorin	−1.19	2.34E-02
Clec3b	C-type lectin domain family 3, member b	−1.16	6.82E-02

wanted to know which cell types in the brain are responsible for the differences in *Npas4* and *Arc* gene expression. Therefore, we performed immunohistological staining in mouse brain sections for Npas4 and Arc protein expression in the hippocampus. We could demonstrate high expression of these proteins in NeuN positive neurons of the granular cell layer in the dentate gyrus (Fig. 6G, arrow). Whereas Arc was exclusively observed in neurons, Npas4 had only minor co-localization with glial cell types (Supplementary Fig. 5A). Furthermore, publically available transcriptome data bases of various mouse CNS cell types revealed that the *Npas4* gene is expressed predominantly in neurons (Supplementary Fig. 5B and Zhang et al., 2014). All together these data confirmed the GO enrichment analysis that alterations in gene expression upon $CD8^+$ T-cell ablation most likely derive from neurons in the hippocampus. Together with our mRNA data this let us conclude that ablation of $CD8^+$ T-cells alters neuronal- and synapse-related gene expression in the hippocampus of APP-PS1 animals, indicating a potential role of $CD8^+$ T-cells in modulating neuronal function within the brain.

4. Discussion

Summarizing our herein shown data, $CD8^+$ T-cells infiltrate the brain parenchyma in an age- and pathology dependent manner. Infiltration started at the age of 10 to 12 months, and with 18–19 months of age APP-PS1 mice had significantly higher numbers of $CD8^+$ T-cells in the hippocampus compared to age-matched WT animals. Also, human post-mortem AD hippocampus samples contained higher numbers of $CD8^+$ T-cells in the parenchyma, which positively correlated with Braak stages. Approaching the functional role of $CD8^+$ T-cells in the brain by ablating the pool of $CD8^+$ T-cells from the blood and brain of APP-PS1 animals, revealed remarkable changes in hippocampal gene expression. Genes related to synaptic plasticity and neuronal function including *Npas4* and *Arc* were significantly higher in APP-PS1 mouse brains lacking $CD8^+$ T-cells. On the cellular level, protein expression of Npas4 and Arc was detected predominantly in neurons, indicating that alterations in gene expression upon $CD8^+$ T-cell ablation mostly derived from neurons. Therefore, we conclude that APP-PS1 brain infiltrating $CD8^+$ T-cells are functionally involved in modulating synaptic plasticity and therefore most likely shape neuronal

Table 5
List of all significantly up-regulated Kegg pathways and their corresponding genes in the hippocampus of APP-PS1 + anti-CD8 mice (sorted after adjusted p-values, adj. p < 0.5).

Pathway	genes	**adj. p-value (< 0.05)**
Circadian entrainment	*Calm3/Adcy1/Grin2c/Per1/Ryr2/Cacna1h/Camk2a/Grin1/Ryr1/Camk2b*	5.38E-04
Calcium signaling pathway	*Calm3/Adcy1/Grin2c/Ryr2/Cacna1h/Camk2a/Pdgfrb/Grin1/Slc8a2/Ryr1/Cacna1a/Orai2/Camk2b*	6.42E-04
Oxytocin signaling pathway	*Mapk7/Calm3/Adcy1/Ryr2/Camk2a/Camkk2/Actb/Ryr1/Pla2g4e/Cacng8/Camk2b*	1.62E-03
Long-term potentiation	*Rps6ka1/Calm3/Adcy1/Grin2c/Camk2a/Grin1/Camk2b*	3.26E-03
Amphetamine addiction	*Calm3/Grin2c/Arc/Camk2a/Grin1/Pdyn/Camk2b*	3.26E-03
MAPK signaling pathway	*Mapk7/Rps6ka1/Srf/Dusp6/Tab1/Nr4a1/Cacna1h/Pdgfrb/Dusp4/Rasgrf1/Cacna1a/Pla2g4e/Cacng8/Dusp7*	5.63E-03
C-type lectin receptor signaling pathway	*Irf9/Calm3/Stat1/Card9/Plk3/Pik3r2/Egr3/Stat2*	8.33E-03
Glutamatergic synapse	*Grik5/Adcy1/Grin2c/Shank3/Grin1/Cacna1a/Shank1/Pla2g4e*	8.33E-03
Insulin secretion	*Adcy1/Ryr2/Camk2a/Trpm4/Abcc8/Gck/Camk2b*	8.33E-03
GnRH signaling pathway	*Mapk7/Calm3/Adcy1/Camk2a/Egr1/Pla2g4e/Camk2b*	9.50E-03
Epstein-Barr virus infection	*Irf9/Tab1/Irf7/Stat1/Pik3r2/Tyk2/Cxcl10/Isg15/Tap1/H2-DMa/Stat2*	1.54E-02
Influenza A	*Irf9/Irf7/Stat1/Actb/Pik3r2/Tyk2/Cxcl10/H2-DMa/Stat2*	1.55E-02
Aldosterone synthesis and secretion	*Calm3/Adcy1/Nr4a1/Cacna1h/Camk2a/Dagla/Camk2b*	1.55E-02
Apelin signaling pathway	*Mef2d/Hdac5/Calm3/Adcy1/Ryr2/Slc8a2/Ryr1/Egr1*	1.99E-02
Axon guidance	*Ephb3/Camk2a/Slit1/Sema4c/Pik3r2/Sema7a/Sema6c/Lrrc4/Camk2b*	2.51E-02
Neurotrophin signaling pathway	*Mapk7/Rps6ka1/Matk/Calm3/Camk2a/Pik3r2/Camk2b*	3.39E-02
Hepatitis C	*Irf9/Irf7/Stat1/Pik3r2/Tyk2/Ifit1/Cxcl10/Stat2*	3.97E-02
Osteoclast differentiation	*Irf9/Tab1/Stat1/Pik3r2/Tyk2/Stat2/Junb*	4.13E-02
Choline metabolism in cancer	*Pdgfrb/Pik3r2/Dgkh/Dgkz/Pla2g4e/Slc44a2*	4.60E-02

activity along AD pathology. Clearly, the exact mechanism is beyond the scope of this study and needs to be further investigated.

The brain is immunologically not isolated from the peripheral immune system as was thought for a long time (reviewed in Aloisi et al., 2000; Gonzalez et al., 2014). In particular in the context of acute damages and chronic inflammatory, but also in chronic neurodegenerative diseases it is by now well established that the blood-brain-barrier is leaky (reviewed in Chodobski et al., 2011; Sweeney et al., 2018a; Sweeney et al., 2018b). Moreover, specific brain compartments as the meninges and the choroid plexus, but also the brain parenchyma itself are highly immune-competent and accommodate a diversity of peripheral derived immune cells (Korin et al., 2017). Peripheral immune cells such as bone-marrow derived monocytes and macrophages enter the CNS and participate for example in amyloid clearance in AD diseased brains (Simard et al., 2006; Stalder et al., 2005; and reviewed in Hohsfield and Humpel, 2015). Moreover, lymphocytes resemble a big proportion of peripheral immune cells that are recruited into the CNS of healthy adult rodents (Korin et al., 2017; and reviewed in Gemechu and Bentivoglio, 2012). Specifically in rodents $CD4^+$ and $CD8^+$ T-cells are reported to infiltrate the CNS in higher numbers during normal brain ageing (Korin et al., 2017; Ritzel et al., 2016) and $CD8^+$ T-cells were also shown to infiltrate the brain upon viral infections (Garber et al., 2019; Wakim et al., 2010). Very recently and similar to our findings, Smolders et al. reported on $CD8^+$ T-cells that populate the human brain and further identified a subpopulation of these cells as tissue resident immune cells expressing CD69 and CD103 with low expression of cytolytic enzymes (Smolders et al., 2018). In neurodegenerative diseases the increased presence of brain T-cells is reported in Parkinsons's disease (PD) (Brochard et al., 2009), amyotrophic lateral sclerosis (ALS) (reviewed in Holmoy, 2008), stroke (reviewed in Arumugam et al., 2005) and in autoimmune diseases as Multiple sclerosis (MS) and animal models for experimental autoimmune encephalomyelitis (Saligrama et al., 2019; and reviewed in Fletcher et al., 2010). In the latter T-cells were found within MS plaques and directly contribute to demyelination in the brain (Peeters et al., 2017; and reviewed in Salou et al., 2015).

In AD and transgenic mouse models for AD the presence and functional relevance of T-cells in the brain is an emerging topic (Baruch et al., 2015; Gate et al., 2020; and reviewed in Schetters et al., 2017). The infiltration of T-cells in human AD brains was first mentioned in 1988 (Rogers et al., 1988; Togo et al., 2002). More recently increased $CD3^+$ T-cell numbers were reported to correlate with Tau pathology rather than amyloidosis in human AD brains (Merlini et al., 2018). Controversially, $CD4^+$ and $CD8^+$ T-cells were mostly described and observed in the brains of transgenic AD animal models with an amyloid plaque rather than Tau pathology (Dansokho et al., 2016; Ferretti et al., 2016). This is in line with our data, since we did not detect increased numbers of $CD8^+$ T-cells in transgenic models for Tau pathology. This, of course might suggest that amyloidosis is involved in triggering T-cell infiltration. The increased amyloid-beta production in the brain is assumed to drive a chronic antigenic stress in the periphery, potentially also leading to peripheral immune cell exhaustion (Monsonego et al., 2001). Most interestingly the number of $CD8^+$ T-cells observed in the mouse brains is often outnumbering $CD4^+$ T-cells (Ferretti et al., 2016).

Several preclinical studies investigated on the beneficial or detrimental role of brain T-cells in AD pathology, however with rather conflicting results (Baruch et al., 2015; Dansokho et al., 2016; Marsh et al., 2016). Some of these studies used immune-deficient mice lacking a wider range of lymphocytes (Marsh et al., 2016), or ablation of $CD3^+$ T-cells in general (Laurent et al., 2017) or of regulatory T-cell populations (Tregs) (Baruch et al., 2015). The results of these studies were quite controversially most likely due to the different T-cell subpopulations addressed and due to the different AD animal models used. Ablation of Tregs in 5xFAD transgenic mice was followed by increased amyloid clearance and reversal of the cognitive decline (Baruch et al., 2015) but at the same time a depletion of overall lymphocyte populations in the same mouse model showed a two-fold increase in amyloid pathology (Marsh et al., 2016). Early depletion of Tregs in APPPS1 mice did not alter plaque pathology but accelerated the onset of cognitive deficits in this mouse model (Dansokho et al., 2016). The majority of these studies in mice were performed at specific ages, i.e. time points of disease development and/or the treatment already started at pre-plaque stages. Therefore, the dynamic of T-cell infiltration and their function within the brain remain unclear. It is still under debate, if T-cells are beneficial or detrimental in AD pathology. Specifically, the $CD8^+$ T-cell population was so far completely ignored in mouse models for amyloidosis.

Our data illustrate the dynamics of $CD8^+$ T-cell infiltration to the brain covering an age spectrum of 3 months up to 26 months old mice. Apparently, age has a huge impact on $CD8^+$ T-cell numbers in the brain. We have chosen a time point, where the cells started to infiltrate typical brain regions of amyloidosis in APP-PS1 mice. At this time point the mice already have fully developed amyloid plaque pathology (Unger et al., 2016). After 4 weeks of $CD8^+$ T-cell depletion we did not observe changes in plaque pathology, suggesting that at this time point the low numbers of brain infiltrating $CD8^+$ T-cells were most likely not primarily contributing to amyloid plaque pathology. However, it is very likely that performing the same experiment in younger or older animals might result in a different outcome on amyloid plaque pathology. This is also in line with our behaviour data, showing no rescue of the cognitive decline at this time point of disease progression. However all being speculative, longitudinal depletion studies would be of great interest in future experiments.

In our study, we primarily focused on $CD8^+$ T-cell populations, which are the 2nd most abundant peripheral lymphocyte population (about 4–5%) within the brain of healthy animals and we did not focus on other peripheral immune cells as for example dendritic cells (about 1%) (Korin et al., 2017). We used a commercially available anti-CD8a antibody (https://bxcell.com/product/m-cd8a-2/), which is frequently used to study the effects of $CD8^+$ T-cell depletion in tumor or cancer biology (Balogh et al., 2018; Moynihan et al., 2016). The T-cell specific receptor CD8 was also demonstrated to be expressed on a subpopulation of thymic and splenic dendritic cells (DCs), that are characterized to be either $CD8^+$ or $CD8^-$ (Vremec et al., 1992). DCs are a very heterogeneous population (reviewed in D'Agostino et al., 2012; Ludewig et al., 2016) and in $CD8a^+$ DCs the $CD8^+$ expression is necessary for their function in cross-presenting antigens via major histocompatibility receptor I to $CD8^+$ T-cells in vivo, thereby inducing $CD8^+$ T-cell responses (den Haan et al., 2000). We cannot exclude possible effects of our anti-CD8a antibody treatment on DC subpopulations, which have been recently reported (Jung et al., 2018). Jung et al. showed that anti-CD8a antibody treatment does barely affect splenic and blood $CD11b^+$ positive DCs in general but $CD8a^+$ DCs are greatly reduced upon treatment (Jung et al., 2018). Jung et al. also demonstrated that there was no effect of anti-CD8 antibody treatment on splenic B-cells. Therefore, we would assume that the possible effects on $CD8a^+$ DCs in our study also result in decreased activation of remaining $CD8^+$ T-cells, but this and possible effects on other immune cell populations is beyond the scope of the herein presented study.

Normally, $CD8^+$ T-cells have cytotoxic effector function eliminating infected target cells or tumor cells (reviewed in Andersen et al., 2006) and their role in neurodegenerative diseases is so far unclear. We were among the first to demonstrate the presence of $CD8^+$ T-cells in APP-PS1 transgenic mice and showed that these cells were in close interaction with microglia cells, forming an immune synapse (Ferretti et al., 2016; Unger et al., 2018a; Unger et al., 2018b). Additionally, we already demonstrated that the $CD8^+$ T-cell population in the APP-PS1 mouse brain is partially controlled by microglia cells, as an ablation of microglia cells for 4 weeks increased the number of brain infiltrating $CD8^+$ T-cells in these mice (Unger et al., 2018b).

In the herein presented work we demonstrate that ageing itself affects the number of $CD8^+$ T-cells found in the brain of WT and of APP-

PS1 mice. This is in line with a recent study demonstrating that increased numbers of clonally expanded T-cells that differ from blood T-cells were found in the neurogenic niche of the SVZ in old mice in close proximity to NSCs (Dulken et al., 2019). Surprisingly, the majority of these T-cells were $CD8^+$ T-cells and not $CD4^+$ T-cells. Interestingly, these neurogenic niche associated $CD8^+$ T-cells negatively affected NSCs via the IFNy signalling pathway (Dulken et al., 2019). Unfortunately, the Dulken study focused only on the SVZ and completely ignored other neurogenic niches such as the hippocampus or also other non-neurogenic brain regions. Concerning the dynamic of T-cell brain infiltration it would also be of great interest to test if these effects also occur in brains of middle aged-mice with lower T-cell numbers in the brain.

Our transcriptome data imply that $CD8^+$ T-cells modulate neuronal- and synapse-related gene expression within the hippocampus. This needs to be seen in the context of our recent study that revealed increased numbers of $CD8^+$ T effector memory $CD45RA^+$ (T_{EMRA}) cells in the blood of AD patients (Gate et al., 2020). These cells negatively correlated with cognition suggesting that the $CD8^+$ T-cell population might affect neuronal functions. Single cell RNA sequencing showed enhanced T-cell receptor (TCR) signaling in these cells. Additionally, clonally expanded $CD8^+$ T_{EMRA} cells were detected in AD CSF samples and some of them were specific for Epstein-Barr virus antigens. Additionally, we demonstrated a spatial co-localization of $CD8^+$ T-cells with neurofilament heavy (NEFH) positive neuronal processes in APP-PS1 mice and in human AD brain tissue, indicating neuronal structures as possible targets in the brain (Gate et al., 2020). In the present study, we substantiate this putative interaction of $CD8^+$ T-cells with neuronal structures on a more molecular/gene expression level, revealing alterations of neuronal- and synapse-related gene expression upon $CD8^+$ T-cell ablation within the hippocampus of APP-PS1 mice. We demonstrate that $CD8^+$ T-cell ablation in APP-PS1 mice increased gene expression of IEGs including *Npas4* and *Arc*.

The transcription factor *Npas4* and the *Arc* gene belong to the family of rapidly up-regulated IEGs that play an important role in synapse development and are involved synaptic processes (reviewed in Kim et al., 2018). Npas4 is a brain specific transcription factor exclusively expressed in neurons, induced by neuronal activity itself and involved in the formation of synapse connections of excitatory and inhibitory neurons as well as memory function (reviewed in Sun and Lin, 2016). Similarly, neuronal activity rapidly regulates expression of *Arc* mRNA that is transcribed and transferred to the site of active synapses in dendrites (Farris et al., 2014; Steward et al., 1998). *Arc* is important for memory consolidation (Guzowski et al., 2000) and Arc knockout mice showed failures in long-term memory formation and changes in LTP (Plath et al., 2006). *Npas4* but also *Arc* mRNA levels were shown to be decreased in the hippocampus of aged-memory impaired mice (Qiu et al., 2016). Dysfunctional levels of Arc protein were detected in the hippocampus of AD transgenic mice (Morin et al., 2016) and Arc is also involved in the generation of amyloid-beta (Wu et al., 2011). In humans, a gene polymorphism in *Arc* is associated with a reduced risk to develop AD (Landgren et al., 2012). *Arc* mRNA expression levels are also highly altered in transgenic AD mouse models (reviewed in Kerrigan and Randall, 2013) and Arc knockout mice show hallmarks related to synapthopathy as similarly observed in AD transgenic mice (Jacobsen et al., 2006; Perez-Cruz et al., 2011; and reviewed in Kerrigan and Randall, 2013). Of note our hippocampal transcriptomic data revealed down-regulated levels of *Npas4* mRNA in APP-PS1 versus WT mice confirming altered synapse-related gene-expression in AD transgenic mice (Supplementary File 1). Our herein performed $CD8^+$ T-cell ablation increased mRNA levels of *Npas4* and *Arc* in the hippocampus of APP-PS1 mice, indicating that $CD8^+$ T-cells are involved in synaptopathy along AD progression in these mice.

Although we do not observe a rescue in the cognitive deficits at this time point of disease progression, our observed changes on mRNA suggest that $CD8^+$ T-cells might be involved in regulating neuronal and/or cognitive function. Similarly, it was already demonstrated in the context of enriched environment and its effect on hippocampus-dependent behaviour and neurogenesis, where $CD8^+$ T-cells were attributed as essential mediators for these beneficial effects on brain plasticity and cognition (Zarif et al., 2018).

In addition to the up-regulated Kegg pathways for LTP and calcium signaling, the $CD8^+$ T-cell ablation in APP-PS1 mice resulted in up-regulated gene pathways related to Influenza A and Epstein-Barr virus infection. Genes involved in these pathways are *Cxcl10* and *Irf7* that were up-regulated and had the highest fold changes in our transcriptomic analysis in APP-PS1 mice lacking $CD8^+$ T-cells. Cxcl10 is a chemokine that was shown to be dysregulated during ageing and increased in the AD brain (Bradburn et al., 2018). Cxcl10 is important in recruiting leukocytes to the brain as was shown by neuronal Cxcl10 expression that recruits $Cxcr3^+$ $CD8^+$ T-cells for clearance in West Nile virus (WNV) encephalitis but recruitment failed in *Cxcl10* knock out mice (Klein et al., 2005). Cxcl10 is also an important ligand for the Cxcr3 receptor on $CD8^+$ effector T-cells in other CNS virus infections (Christensen et al., 2006) and Cxcl10 expression in cancer associated to Epstein-Barr virus infection is controversially discussed (Jing et al., 2018; Li et al., 2007; Teichmann et al., 2005). In accordance with our data, we can so far only speculate if neurons in APP-PS1 mice in the absence of $CD8^+$ T-cells possibly increase the gene expression of *Cxcl10* to somehow recruit other leukocytes to the brain.

Irf7 is an important transcription factor and regulator of type 1 interferons that was shown to translocate to the nucleus upon activation (Honda et al., 2005; and reviewed in Ning et al., 2011). It was primarily shown to be directly activated by Epstein-Barr virus (EBV) protein LMP1 (Zhang and Pagano, 2000). In AD, patients carrying an *Irf7* polymorphisms had higher anti-herpes simplex virus 1 antibody titers indicating altered immune responses to viral infections (Costa et al., 2017).

Observing a modulation in expression of viral infection-related gene sets due to $CD8^+$ T-cell ablation is of great interest as we could previously demonstrate that EBV-specific T-cell clones are present in the CSF of AD patients (Gate et al., 2020). However, one has to be careful that this data is not enough to clearly demonstrate a link between Epstein-Barr infection and AD, but it is discussed that EBV infection is a possible risk factor for AD development (Carbone et al., 2014; Tzeng et al., 2018). A role of $CD8^+$ T-cells in promoting microglia-mediated synaptic elimination is already described in virus infected brains (Garber et al., 2019), however the function of $CD8^+$ T-cells in the brain of AD patients is so far not understood.

Therefore, the herein shown data reveal new insights on the presence of CNS-specific $CD8^+$ T-cells in AD pathology and let speculate on their possible function in the brain parenchyma. The current understanding of T-cells in the brain especially in contact with microglia as antigen presenting cells (APCs) under chronic neurodegenerative conditions is that microglia T-cell crosstalk takes place as two-step process: first initiated by peripheral APCs in peripheral immune organs, e.g. in the lymph nodes, and is followed by local restimulation through microglia in the CNS, which modulate T-cell phenotypes and T-cell responses in the brain (reviewed in Schetters et al., 2017). We previously could demonstrate the interaction of $CD8^+$ T-cells with brain resident microglia cells in APP-PS1 transgenic mice (Unger et al., 2018b). Microglia cells might not only alter $CD8^+$ T-cell function in the CNS but also CNS-specific $CD8^+$ T-cells possibly influence microglia phenotypes and therefore might shape neuroinflammation and as a result also synaptic plasticity. However, the antigens that are presented to T-cells in the brain of AD transgenic mice are so far completely unknown (reviewed in Schetters et al., 2017).

If the attack of $CD8^+$ T-cells on neurons or neuronal structures in AD is directly causing altered synaptic plasticity or if the presence of $CD8^+$ T-cells in the brain modulates microglia and their function in synaptic stripping is so far not known. However, in virus infection models as the viral déjà vu rLCMV mouse model, a model recapitulating

features of Rasmussen's encephalitis (RE), an interaction of $CD8^+$ T-cells with neurons and microglia was demonstrated (Di Liberto et al., 2018). In this study, Di Liberto G. et al. showed that brain infiltrating $CD8^+$ T-cells located at sites of virus infected neurons and stimulated neuronal Stat1 phosphorylation via IFNy signaling. As consequence neurons released the chemokine CCL2 leading to apposition of phagocytes as microglia and macrophages, which subsequently drive synaptic loss (Di Liberto et al., 2018). Most interestingly, our herein presented ablation of $CD8^+$ T-cells in APP-PS1 mice resulted in an up-regulation of *Stat1* mRNA in the hippocampus. The study by Di Liberto G. et al. demonstrated that neurons coordinate synapse stripping by signaling to microglia cells and that this interaction is out of balance when the brain is under $CD8^+$ T-cell attack. If this mechanism of T-cell-microglia-neuron interaction is similar in AD pathology and if $CD8^+$ T-cells in the AD brain have similar functions in orchestrating synaptic plasticity is so far completely unknown. To stress this point even further, the mere MHCI restricted cell-to-cell contact of $CD8^+$ T-cells with neurons in the brain can cause neuronal "shutdown" and silencing of electrical signals and was already demonstrated in vitro and ex vivo on hippocampal slices (Meuth et al., 2009; and reviewed in Ehling et al., 2015). However, if brain $CD8^+$ T-cells in AD are capable to silence neurons and if the ablation of these cells and the resulting change on synapse-related gene expression also results in functional responses needs to be further investigated in the future.

5. Conclusion

Our herein shown data open new insights on the contribution of the adaptive immune system to AD pathology. $CD8^+$ T-cells start to infiltrate AD brains and are possible new cellular players that contribute to neuronal and synaptic alterations. Understanding the exact functional relevance of $CD8^+$ T-cell subsets in the brain of AD patients might open new ways to treat AD pathology by modulating the immune system. Further investigations on T-cell-neuron interactions in the brain need to be performed to characterize the function of these cells in more detail. The herein presented data show new aspects on the adaptive immune responses that take place in AD pathology and are therefore important for the broad field of AD research.

6. Availability of data and material

Authors declare availability of data and material upon request. Additionally, the RNAseq data discussed in this publication have been deposited in NCBI's Gene Expression Omnibus (Edgar et al., 2002) and are accessible through GEO Series accession number **GSE149661** (https://www.ncbi.nlm.nih.gov/geo/query/acc.cgi?acc=GSE149661).

Ethical approval and consent to participate

Human post-mortem brain samples were obtained from the Newcastle Brain Tissue Resource (NBTR) in accordance with Newcastle University ethics board and ethical approval awarded by The Joint Ethics Committee of Newcastle and North Tyneside Health Authority (reference: 08/H0906/136). Animal care, handling, genotyping and experiments were approved by local ethical committees (BMWFW-66.019/0011-WF/V/3b/2016 and BMBWF-66.019/0005-V/3b/2018).

Author contributions

MU planned and conducted the animal experiment, performed flow cytometry and histological analysis and wrote the manuscript. EL helped with the animal experiment and performed mouse behaviour, histology and flow cytometry analysis. LS performed human and mouse histology, gene expression analysis by qPCR and cytokine analysis in mouse blood sera. RP performed all bioinformatics analyses of the RNAseq data. BA helped with mouse histology and HM helped with animal perfusion, sample processing and performed qPCR. BHP provided tissue of Tau pathology mice. TMW was involved in critical revision of the manuscript together with JA, who provided human post-mortem brain specimen. MTH provided additional tissue of the APP-PS1 mice. LA is the principle investigator and was involved in the experimental designs, in critical revision and drafting of the manuscript.

Declaration of Competing Interest

The authors declare that they have no known competing financial interests or personal relationships that could have appeared to influence the work reported in this paper.

Acknowledgments

The authors thank the flow cytometry and microscopy core facility of SCI-TReCS (Spinal Cord Injury and Tissue Regeneration Center Salzburg). Furthermore, we thank Pia Zaunmair for her help with the animal breeding.

Funding

This work was supported by the FWF Special Research Program (SFB) F44 (F4413-B23) "Cell Signaling in Chronic CNS Disorders", FWF Project P 31362-B34, and through funding from the European Union's Seventh Framework Program (FP7/2007-2013) under grant agreements n° HEALTH-F2-2011-278850 (INMiND).

Funding bodies did not influence the design of the study and collection, analysis, interpretation of data, and writing of the manuscript.

Appendix A. Supplementary data

Supplementary data to this article can be found online at https://doi.org/10.1016/j.bbi.2020.05.070.

References

Aloisi, F., Ria, F., Adorini, L., 2000. Regulation of T-cell responses by CNS antigen-presenting cells: different roles for microglia and astrocytes. Immunol. Today 21, 141–147.
Anders, S., Pyl, P.T., Huber, W., 2015. HTSeq–a Python framework to work with high-throughput sequencing data. Bioinformatics 31, 166–169.
Andersen, M.H., et al., 2006. Cytotoxic T cells. J, Invest. Dermatol. 126, 32–41.
Andorfer, C., et al., 2003. Hyperphosphorylation and aggregation of tau in mice expressing normal human tau isoforms. J. Neurochem. 86, 582–590.
Andrews, S., 2010. FastQC: A Quality Control Tool for High Throughput Sequence Data [Online].
Arumugam, T.V., Granger, D.N., Mattson, M.P., 2005. Stroke and T-cells. Neuromolecular Med. 7, 229–242.
Balogh, K.N., Templeton, D.J., Cross, J.V., 2018. Macrophage Migration Inhibitory Factor protects cancer cells from immunogenic cell death and impairs anti-tumor immune responses. PLoS ONE 13, e0197702.
Baruch, K., Schwartz, M., 2013. CNS-specific T cells shape brain function via the choroid plexus. Brain Behav. Immun. 34, 11–16.
Baruch, K., et al., 2015. Breaking immune tolerance by targeting Foxp3(+) regulatory T cells mitigates Alzheimer's disease pathology. Nat. Commun. 6, 7967.
Becher, B., Antel, J.P., 1996. Comparison of phenotypic and functional properties of immediately ex vivo and cultured human adult microglia. Glia 18, 1–10.
Bennett, M.L., et al., 2016. New tools for studying microglia in the mouse and human CNS. Proc. Natl. Acad. Sci. U.S.A. 113, E1738–E1746.
Braak, H., Braak, E., 1991. Neuropathological stageing of Alzheimer-related changes. Acta Neuropathol. 82, 239–259.
Braak, H., et al., 2006. Staging of Alzheimer disease-associated neurofibrillary pathology using paraffin sections and immunocytochemistry. Acta Neuropathol. 112, 389–404.
Bradburn, S., et al., 2018. Dysregulation of C-X-C motif ligand 10 during aging and association with cognitive performance. Neurobiol. Aging 63, 54–64.
Brochard, V., et al., 2009. Infiltration of CD4+ lymphocytes into the brain contributes to neurodegeneration in a mouse model of Parkinson disease. J. Clin. Invest. 119, 182–192.
Bromley-Brits, K., Deng, Y., Song, W., 2011. Morris water maze test for learning and memory deficits in Alzheimer's disease model mice. J. Vis. Exp.
Carbone, I., et al., 2014. Herpes virus in Alzheimer's disease: relation to progression of the disease. Neurobiol. Aging 35, 122–129.
Chodobski, A., Zink, B.J., Szmydynger-Chodobska, J., 2011. Blood-brain barrier

pathophysiology in traumatic brain injury. Transl Stroke Res. 2, 492–516.
Christensen, J.E., et al., 2006. CXCL10 is the key ligand for CXCR3 on CD8+ effector T cells involved in immune surveillance of the lymphocytic choriomeningitis virus-infected central nervous system. J. Immunol. 176, 4235–4243.
Costa, A.S., et al., 2017. Modulation of immune responses to herpes simplex virus type 1 by IFNL3 and IRF7 polymorphisms: a study in Alzheimer's disease. J. Alzheimers Dis. 60, 1055–1063.
D'Agostino, P.M., et al., 2012. Brain dendritic cells: biology and pathology. Acta Neuropathol. 124, 599–614.
Dansokho, C., et al., 2016. Regulatory T cells delay disease progression in Alzheimer-like pathology. Brain 139, 1237–1251.
den Haan, J.M., Lehar, S.M., Bevan, M.J., 2000. CD8(+) but not CD8(-) dendritic cells cross-prime cytotoxic T cells in vivo. J. Exp. Med. 192, 1685–1696.
Di Liberto, G., et al., 2018. Neurons under T cell attack coordinate phagocyte-mediated synaptic stripping. Cell 175 (458–471), e19.
Dulken, B.W., et al., 2019. Single-cell analysis reveals T cell infiltration in old neurogenic niches. Nature 571, 205–210.
Edgar, R., Domrachev, M., Lash, A.E., 2002. Gene expression omnibus: NCBI gene expression and hybridization array data repository. Nucleic Acids Res. 30, 207–210.
Ehling, P., et al., 2015. CD8(+) T cell-mediated neuronal dysfunction and degeneration in limbic encephalitis. Front. Neurol. 6, 163.
Farris, S., et al., 2014. Selective localization of arc mRNA in dendrites involves activity- and translation-dependent mRNA degradation. J. Neurosci. 34, 4481–4493.
Ferretti, M.T., et al., 2016. T-cell brain infiltration and immature antigen-presenting cells in transgenic models of Alzheimer's disease-like cerebral amyloidosis. Brain Behav. Immun. 54, 211–225.
Fletcher, J.M., et al., 2010. T cells in multiple sclerosis and experimental autoimmune encephalomyelitis. Clin. Exp. Immunol. 162, 1–11.
Flunkert, S., et al., 2013. Elevated levels of soluble total and hyperphosphorylated tau result in early behavioral deficits and distinct changes in brain pathology in a new tau transgenic mouse model. Neurodegener Dis. 11, 194–205.
Ford, A.L., et al., 1995. Normal adult ramified microglia separated from other central nervous system macrophages by flow cytometric sorting. Phenotypic differences defined and direct ex vivo antigen presentation to myelin basic protein-reactive CD4+ T cells compared. J. Immunol. 154, 4309–4321.
Fu, R., et al., 2014. Phagocytosis of microglia in the central nervous system diseases. Mol. Neurobiol. 49, 1422–1434.
Garber, C., et al., 2019. T cells promote microglia-mediated synaptic elimination and cognitive dysfunction during recovery from neuropathogenic flaviviruses. Nat. Neurosci. 22, 1276–1288.
Garcia-Alloza, M., et al., 2006. Characterization of amyloid deposition in the APPswe/PS1dE9 mouse model of Alzheimer disease. Neurobiol. Dis. 24, 516–524.
Gate, D., et al., 2010. Macrophages in Alzheimer's disease: the blood-borne identity. J Neural Transm (Vienna). 117, 961–970.
Gate, D., et al., 2020. Clonally expanded CD8 T cells patrol the cerebrospinal fluid in Alzheimer's disease. Nature 577, 399–404.
Gemechu, J.M., Bentivoglio, M., 2012. T cell recruitment in the brain during normal aging. Front. Cell. Neurosci. 6, 38.
Goedert, M., Spillantini, M.G., 2006. A century of Alzheimer's disease. Science 314, 777–781.
Gonzalez, H., et al., 2014. Neuroimmune regulation of microglial activity involved in neuroinflammation and neurodegenerative diseases. J. Neuroimmunol. 274, 1–13.
Gotz, J., et al., 2007. A decade of tau transgenic animal models and beyond. Brain Pathol. 17, 91–103.
Guzowski, J.F., et al., 2000. Inhibition of activity-dependent arc protein expression in the rat hippocampus impairs the maintenance of long-term potentiation and the consolidation of long-term memory. J. Neurosci. 20, 3993–4001.
Hamilton, A., Holscher, C., 2012. The effect of ageing on neurogenesis and oxidative stress in the APP(swe)/PS1(deltaE9) mouse model of Alzheimer's disease. Brain Res. 1449, 83–93.
Heneka, M.T., et al., 2015. Neuroinflammation in Alzheimer's disease. Lancet Neurol. 14, 388–405.
Heppner, F.L., Ransohoff, R.M., Becher, B., 2015. Immune attack: the role of inflammation in Alzheimer disease. Nat. Rev. Neurosci. 16, 358–372.
Hohsfield, L.A., Humpel, C., 2015. Migration of blood cells to beta-amyloid plaques in Alzheimer's disease. Exp. Gerontol. 65, 8–15.
Holmoy, T., 2008. T cells in amyotrophic lateral sclerosis. Eur. J. Neurol. 15, 360–366.
Honda, K., et al., 2005. IRF-7 is the master regulator of type-I interferon-dependent immune responses. Nature 434, 772–777.
Jacobsen, J.S., et al., 2006. Early-onset behavioral and synaptic deficits in a mouse model of Alzheimer's disease. Proc. Natl. Acad. Sci. U.S.A. 103, 5161–5166.
Jankowsky, J.L., et al., 2001. Co-expression of multiple transgenes in mouse CNS: a comparison of strategies. Biomol. Eng. 17, 157–165.
Jankowsky, J.L., et al., 2004. Mutant presenilins specifically elevate the levels of the 42 residue beta-amyloid peptide in vivo: evidence for augmentation of a 42-specific gamma secretase. Hum. Mol. Genet. 13, 159–170.
Jevtic, S., et al., 2017. The role of the immune system in Alzheimer disease: etiology and treatment. Ageing Res Rev. 40, 84–94.
Jing, J.J., et al., 2018. Key elements involved in Epstein-Barr virus-associated gastric cancer and their network regulation. Cancer Cell Int. 18, 146.
Jung, S.R., et al., 2018. Collateral damage: what effect does anti-CD4 and Anti-CD8alpha antibody-mediated depletion have on leukocyte populations? J. Immunol. 201, 2176–2186.
Kerrigan, T.L., Randall, A.D., 2013. A new player in the "synaptopathy" of Alzheimer's disease – arc/arg 3.1. Front. Neurol. 4, 9.
Kettenmann, H., et al., 2011. Physiology of microglia. Physiol. Rev. 91, 461–553.
Kim, S., Kim, H., Um, J.W., 2018. Synapse development organized by neuronal activity-regulated immediate-early genes. Exp. Mol. Med. 50, 11.
Klein, R.S., et al., 2005. Neuronal CXCL10 directs CD8+ T-cell recruitment and control of West Nile virus encephalitis. J. Virol. 79, 11457–11466.
Kniewallner, K.M., Foidl, B.M., Humpel, C., 2018. Platelets isolated from an Alzheimer mouse damage healthy cortical vessels and cause inflammation in an organotypic ex vivo brain slice model. Sci. Rep. 8, 15483.
Kniewallner, K.M., et al., 2020. Platelets in amyloidogenic mice are activated and invade the brain. Front. Neurosci. 14, 129.
Korin, B., et al., 2017. High-dimensional, single-cell characterization of the brain's immune compartment. Nat. Neurosci. 20, 1300–1309.
Krabbe, G., et al., 2013. Functional impairment of microglia coincides with Beta-amyloid deposition in mice with Alzheimer-like pathology. PLoS ONE 8, e60921.
Laky, K., Kruisbeek, A.M., 2016. In vivo depletion of T lymphocytes. Curr Protoc Immunol. 113, 4 1, 1–9.
Landgren, S., et al., 2012. A novel ARC gene polymorphism is associated with reduced risk of Alzheimer's disease. J. Neural Transm. (Vienna) 119, 833–842.
Langmead, B., Salzberg, S.L., 2012. Fast gapped-read alignment with Bowtie 2. Nat. Methods 9, 357–359.
Laurent, C., et al., 2017. Hippocampal T cell infiltration promotes neuroinflammation and cognitive decline in a mouse model of tauopathy. Brain 140, 184–200.
Li, J., et al., 2007. Expression of immune-related molecules in primary EBV-positive Chinese nasopharyngeal carcinoma: associated with latent membrane protein 1 (LMP1) expression. Cancer Biol. Ther. 6, 1997–2004.
Livak, K.J., Schmittgen, T.D., 2001. Analysis of relative gene expression data using real-time quantitative PCR and the 2(-Delta Delta C(T)) method. Methods 25, 402–408.
Love, M.I., Huber, W., Anders, S., 2014. Moderated estimation of fold change and dispersion for RNA-seq data with DESeq2. Genome Biol. 15, 550.
Ludewig, P., et al., 2016. Dendritic cells in brain diseases. Biochim. Biophys. Acta, Mol. Cell. Biol. Lipids 1862, 352–367.
Marschallinger, J., et al., 2015. The L-type calcium channel Cav1.3 is required for proper hippocampal neurogenesis and cognitive functions. Cell Calcium 58, 606–616.
Marsh, S.E., et al., 2016. The adaptive immune system restrains Alzheimer's disease pathogenesis by modulating microglial function. Proc. Natl. Acad. Sci. U.S.A. 113, E1316–E1325.
McKeith, I.G., et al., 2005. Diagnosis and management of dementia with Lewy bodies: third report of the DLB Consortium. Neurology 65, 1863–1872.
Meadowcroft, M.D., et al., 2009. MRI and histological analysis of beta-amyloid plaques in both human Alzheimer's disease and APP/PS1 transgenic mice. J. Magn. Reson. Imaging 29, 997–1007.
Merlini, M., et al., 2018. Extravascular CD3+ T cells in brains of Alzheimer disease patients correlate with tau but not with amyloid pathology: an immunohistochemical study. Neurodegener. Dis. 18, 49–56.
Meuth, S.G., et al., 2009. Cytotoxic CD8+ T cell-neuron interactions: perforin-dependent electrical silencing precedes but is not causally linked to neuronal cell death. J. Neurosci. 29, 15397–15409.
Mirra, S.S., et al., 1991. The consortium to establish a registry for Alzheimer's disease (CERAD). Part II. Standardization of the neuropathologic assessment of Alzheimer's disease. Neurology. 41, 479–486.
Monsonego, A., et al., 2001. Immune hyporesponsiveness to amyloid beta-peptide in amyloid precursor protein transgenic mice: implications for the pathogenesis and treatment of Alzheimer's disease. Proc. Natl. Acad. Sci. U.S.A. 98, 10273–10278.
Montine, T.J., et al., 2012. National Institute on Aging-Alzheimer's Association guidelines for the neuropathologic assessment of Alzheimer's disease: a practical approach. Acta Neuropathol. 123, 1–11.
Morin, J.P., et al., 2016. Spatial memory impairment is associated with intraneural amyloid-beta immunoreactivity and dysfunctional arc expression in the hippocampal-CA3 region of a transgenic mouse model of Alzheimer's disease. J. Alzheimers Dis. 51, 69–79.
Morris, R.G.M., 1981. Spatial localization does not require the presence of local cues. Learn. Motiv. 12, 239–260.
Moynihan, K.D., et al., 2016. Eradication of large established tumors in mice by combination immunotherapy that engages innate and adaptive immune responses. Nat. Med. 22, 1402–1410.
Ning, S., Pagano, J.S., Barber, G.N., 2011. IRF7: activation, regulation, modification and function. Genes Immun. 12, 399–414.
Peeters, L.M., et al., 2017. Cytotoxic CD4+ T cells drive multiple sclerosis progression. Front. Immunol. 8, 1160.
Perez-Cruz, C., et al., 2011. Reduced spine density in specific regions of CA1 pyramidal neurons in two transgenic mouse models of Alzheimer's disease. J. Neurosci. 31, 3926–3934.
Philipson, O., et al., 2010. Animal models of amyloid-beta-related pathologies in Alzheimer's disease. FEBS J. 277, 1389–1409.
Plath, N., et al., 2006. Arc/Arg3.1 is essential for the consolidation of synaptic plasticity and memories. Neuron 52, 437–444.
Prokop, S., et al., 2015. Impact of peripheral myeloid cells on amyloid-beta pathology in Alzheimer's disease-like mice. J. Exp. Med. 212, 1811–1818.
Qiu, J., et al., 2016. Decreased Npas4 and Arc mRNA levels in the hippocampus of aged memory-impaired wild-type but not memory preserved 11beta-HSD1 Deficient mice. J. Neuroendocrinol. 28.
Ritzel, R.M., et al., 2016. Age-associated resident memory CD8 T cells in the central nervous system are primed to potentiate inflammation after ischemic brain injury. J. Immunol. 196, 3318–3330.
Rogers, J., et al., 1988. Expression of immune system-associated antigens by cells of the human central nervous system: relationship to the pathology of Alzheimer's disease. Neurobiol. Aging 9, 339–349.

Rotheneichner, P., et al., 2017. Tamoxifen activation of cre-recombinase has no persisting effects on adult neurogenesis or learning and anxiety. Front. Neurosci. 11, 27.
Saligrama, N., et al., 2019. Opposing T cell responses in experimental autoimmune encephalomyelitis. Nature 572, 481–487.
Salou, M., et al., 2015. Involvement of CD8(+) T cells in multiple sclerosis. Front. Immunol. 6, 604.
Schetters, S.T.T., et al., 2017. Neuroinflammation: microglia and T cells get ready to tango. Front. Immunol. 8, 1905.
Schnell, S.A., Staines, W.A., Wessendorf, M.W., 1999. Reduction of lipofuscin-like autofluorescence in fluorescently labeled tissue. J. Histochem. Cytochem. 47, 719–730.
Selkoe, D.J., Hardy, J., 2016. The amyloid hypothesis of Alzheimer's disease at 25 years. EMBO Mol. Med. 8, 595–608.
Serrano-Pozo, A., et al., 2011. Neuropathological alterations in Alzheimer disease. Cold Spring Harb Perspect Med. 1, a006189.
Simard, A.R., et al., 2006. Bone marrow-derived microglia play a critical role in restricting senile plaque formation in Alzheimer's disease. Neuron 49, 489–502.
Smolders, J., et al., 2018. Tissue-resident memory T cells populate the human brain. Nat. Commun. 9, 4593.
Stalder, A.K., et al., 2005. Invasion of hematopoietic cells into the brain of amyloid precursor protein transgenic mice. J. Neurosci. 25, 11125–11132.
Steward, O., et al., 1998. Synaptic activation causes the mRNA for the IEG Arc to localize selectively near activated postsynaptic sites on dendrites. Neuron 21, 741–751.
Sun, X., Lin, Y., 2016. Npas4: linking neuronal activity to memory. Trends Neurosci. 39, 264–275.
Supek, F., et al., 2011. REVIGO summarizes and visualizes long lists of gene ontology terms. PLoS ONE 6, e21800.
Sweeney, M.D., et al., 2018a. The role of brain vasculature in neurodegenerative disorders. Nat. Neurosci. 21, 1318–1331.
Sweeney, M.D., Sagare, A.P., Zlokovic, B.V., 2018b. Blood-brain barrier breakdown in Alzheimer disease and other neurodegenerative disorders. Nat. Rev. Neurol. 14, 133–150.
Teichmann, M., et al., 2005. Expression of the interferon-inducible chemokine IP-10 (CXCL10), a chemokine with proposed anti-neoplastic functions, in Hodgkin lymphoma and nasopharyngeal carcinoma. J. Pathol. 206, 68–75.
Thal, D.R., et al., 2002. Phases of A beta-deposition in the human brain and its relevance for the development of AD. Neurology 58, 1791–1800.
Theriault, P., ElAli, A., Rivest, S., 2015. The dynamics of monocytes and microglia in Alzheimer's disease. Alzheimers Res. Ther. 7, 41.
Togo, T., et al., 2002. Occurrence of T cells in the brain of Alzheimer's disease and other neurological diseases. J. Neuroimmunol. 124, 83–92.
Tzeng, N.S., et al., 2018. Anti-herpetic medications and reduced risk of dementia in patients with herpes simplex virus infections-a nationwide, population-based cohort study in Taiwan. Neurotherapeutics 15, 417–429.
Unger, M.S., et al., 2016. Early changes in hippocampal neurogenesis in transgenic mouse models for Alzheimer's Disease. Mol. Neurobiol. 53, 5796–5806.
Unger, M.S., et al., 2018a. Doublecortin expression in CD8+ T-cells and microglia at sites of amyloid-beta plaques: a potential role in shaping plaque pathology? Alzheimers Dement. 14, 1022–1037.
Unger, M.S., et al., 2018b. Microglia prevent peripheral immune cell invasion and promote an anti-inflammatory environment in the brain of APP-PS1 transgenic mice. J. Neuroinflamm. 15, 274.
Vremec, D., et al., 1992. The surface phenotype of dendritic cells purified from mouse thymus and spleen: investigation of the CD8 expression by a subpopulation of dendritic cells. J. Exp. Med. 176, 47–58.
Wakim, L.M., Woodward-Davis, A., Bevan, M.J., 2010. Memory T cells persisting within the brain after local infection show functional adaptations to their tissue of residence. Proc. Natl. Acad. Sci. U.S.A. 107, 17872–17879.
Wu, J., et al., 2011. Arc/Arg3.1 regulates an endosomal pathway essential for activity-dependent beta-amyloid generation. Cell 147, 615–628.
Wyss-Coray, T., 2006. Inflammation in Alzheimer disease: driving force, bystander or beneficial response? Nat. Med. 12, 1005–1015.
Wyss-Coray, T., Rogers, J., 2012. Inflammation in Alzheimer disease-a brief review of the basic science and clinical literature. Cold Spring Harb. Perspect Med. 2, a006346.
Yu, G., et al., 2012. clusterProfiler: an R package for comparing biological themes among gene clusters. OMICS 16, 284–287.
Zarif, H., et al., 2018. CD8(+) T cells are essential for the effects of enriched environment on hippocampus-dependent behavior, hippocampal neurogenesis and synaptic plasticity. Brain Behav. Immun. 69, 235–254.
Zenaro, E., et al., 2015. Neutrophils promote Alzheimer's disease-like pathology and cognitive decline via LFA-1 integrin. Nat. Med. 21, 880–886.
Zhang, L., Pagano, J.S., 2000. Interferon regulatory factor 7 is induced by Epstein-Barr virus latent membrane protein 1. J. Virol. 74, 1061–1068.
Zhang, Y., et al., 2014. An RNA-sequencing transcriptome and splicing database of glia, neurons, and vascular cells of the cerebral cortex. J. Neurosci. 34, 11929–11947.